



Monte Carlo study of an improved clock model in three dimensions

Martin Hasenbusch *

Institut für Theoretische Physik, Universität Heidelberg, Philosophenweg 19, 69120 Heidelberg, Germany

 (Received 18 October 2019; revised manuscript received 8 December 2019; published 26 December 2019)

We study a generalized clock model on the simple cubic lattice. The parameter of the model can be tuned such that the amplitude of the leading correction to scaling vanishes. In the main part of the study, we simulate the model with Z_8 symmetry. At the transition, with increasing length scale, $O(2)$ symmetry emerges. We perform Monte Carlo simulations using a hybrid of local Metropolis and cluster algorithms of lattices with a linear size up to $L = 512$. The field variable requires less memory and the updates are faster than for a model with $O(2)$ symmetry at the microscopic level. Our finite-size scaling analysis yields accurate estimates for the critical exponents of the three-dimensional XY -universality class. In particular, we get $\eta = 0.03810(8)$, $\nu = 0.67169(7)$, and $\omega = 0.789(4)$. Furthermore, we obtain estimates for fixed point values of phenomenological couplings and critical temperatures.

DOI: [10.1103/PhysRevB.100.224517](https://doi.org/10.1103/PhysRevB.100.224517)

I. INTRODUCTION

In the neighborhood of a second-order phase transition, thermodynamic quantities diverge, following power laws. For example, the correlation length ξ behaves as

$$\xi = a_{\pm}|t|^{-\nu} (1 + b_{\pm}|t|^{\theta} + ct + \dots), \quad (1)$$

where $t = (T - T_c)/T_c$ is the reduced temperature. The subscript \pm of the amplitudes a_{\pm} and b_{\pm} indicates the high-temperature (+) and the low-temperature (−) phase, respectively. Second-order phase transitions are grouped into universality classes. For all transitions within such a class, critical exponents like ν assume the identical value. These power laws are affected by corrections. There are nonanalytic or confluent and analytic ones. The leading corrections are explicitly given in Eq. (1). Also, correction exponents such as $\theta = \omega\nu$ are universal. For the system discussed here, $\theta \approx 0.5$. Amplitudes such as a_{\pm} and b_{\pm} depend on the microscopic details of the system. However, certain combinations, called amplitude ratios, assume universal values. Universality classes are characterized by the symmetry properties of the order parameter at criticality, the range of the interaction, and the spacial dimension of the system. For reviews on critical phenomena, see, for example, [1–4].

Note that in general the symmetry properties of the order parameter cannot be naively inferred from the microscopic properties of the system. In particular, a symmetry might emerge that is not present in the classical Hamiltonian. For example, in the model studied here, the symmetry is enhanced from Z_N to $O(2)$ at the critical point. At the $O(2)$ -invariant Wilson-Fisher fixed point in three dimensions, a perturbation that breaks the $O(2)$ invariance down to Z_N invariance is irrelevant in the sense of the renormalization group (RG) for $N \geq 4$. See Ref. [5] and references therein. Monte Carlo studies have shown that the transition of N -state clock models

on the simple cubic lattice are in the domain of attraction of the $O(2)$ -invariant fixed point for $N \geq 5$. See, for example, Ref. [6]. The major part of our simulations are performed for $N = 8$. The related RG exponent takes the value $\nu_{N=8} = -5.278(9)$; see Table II of Ref. [5]. Therefore, the deviations from $O(2)$ invariance rapidly vanish with increasing lattice size and can be safely ignored in the finite-size scaling analysis at the critical point. The Z_N -invariant perturbation is dangerously irrelevant. In the low-temperature phase, in the thermodynamic limit, the spontaneous magnetization might only assume one of the N directions that are preferred by the Hamiltonian. See, for example, Ref. [7] and references therein. In the present work, we focus on the critical point and consider a model with Z_N symmetry, mainly for technical reasons. Less memory is needed to store the configurations and the updates require less computer processing time than for a model with $O(2)$ symmetry.

The three-dimensional XY -universality class has attracted much attention, since the λ transition of ${}^4\text{He}$, which is well studied experimentally, is supposed to share this universality class. The most accurate result for the exponent α of the specific heat is obtained from an experiment under the condition of microgravity [8–10]:

$$\alpha = -0.0127(3), \quad (2)$$

which corresponds to $\nu = (2 - \alpha)/d = 0.6709(1)$.

The three-dimensional XY -universality class has been studied by using various theoretical approaches. For example, field theoretic methods, high- and low-temperature series expansions, and Monte Carlo simulations of lattice models. A few representative results for critical exponents are given in Table I. Note that other critical exponents can be obtained from ν and η by using scaling relations. For more comprehensive collections, see Table I of Ref. [15], Table 19 of Ref. [4], or Table I of Ref. [13]. Recently, great progress has been achieved by using the so-called conformal bootstrap method. In particular, in the case of the three-dimensional Ising universality class, the accuracy that has been reached for

*M.Hasenbusch@thphys.uni-heidelberg.de

TABLE I. A few representative results for the critical exponents ν , η , and ω for the universality class of the three-dimensional XY model obtained by various theoretical methods. MC+HT means that Monte Carlo simulations and the analysis of high-temperature expansions have been combined to analyze the lattice models under consideration.

| Ref. | Method | Year | ν | η | ω |
|--------------|----------------------|------|-------------|-------------|-----------|
| [11] | ϵ expansion | 1998 | 0.6680(35) | 0.0380(50) | 0.802(18) |
| [11] | 3D expansion | 1998 | 0.6703(15) | 0.0354(25) | 0.789(11) |
| [12] | MC+HT | 2006 | 0.6717(1) | 0.0381(2) | 0.785(20) |
| [13] | MC | 2019 | 0.67183(18) | 0.03853(48) | 0.77(13) |
| [14] | Conformal bootstrap | 2016 | 0.6719(11) | 0.03852(64) | |
| Present work | MC | 2019 | 0.67169(7) | 0.03810(8) | 0.789(4) |

critical exponents clearly surpasses that of other theoretical methods. See Ref. [16] and references therein. For the XY and the $O(3)$ universality classes in three dimensions, the results obtained so far are less precise. The estimates given in Table I are derived from the numbers for the scaling dimensions Δ_ϕ and Δ_s given in Ref. [14]. In the last row of Table I, we report as preview the results of the present work. We fully confirm Ref. [12], the discrepancy with the experiment [8–10] remains.

An important feature of Refs. [12,15] is that improved models are studied. One considers models that have one parameter in addition to the inverse temperature and the external field. On the critical line, the amplitude b_\pm of leading corrections to scaling, Eq. (1), depends on this parameter. If there exists a value of the parameter with $b_\pm = 0$, RG theory predicts that the same holds for all quantities that are singular at the transition. In the following, we shall call a model with $b_\pm = 0$ an improved model. The idea had been exploited first by using high-temperature series expansions of such models [17,18]. For early Monte Carlo simulations of improved models sharing the universality class of the three-dimensional Ising model, see, for example, Refs. [19–21].

In the present work, we study a generalization of the N -state clock model, which is closely related with the ddXY model that has been studied in Refs. [12,15]. In addition to the N values on the unit circle, the field variable might take the value (0,0) in the center of the circle. We refer to this model as the $(N+1)$ -state clock model. Its precise definition is given in Sec. II below.

We study the model by using finite-size scaling (FSS) [22]. The outline of the study builds upon our previous work on critical phenomena; see, for example, Refs. [12,15,21,23–26], to give only a few. An important feature of these studies is that in addition to the Binder cumulant [27], other dimensionless ratios like the second-moment correlation length over the linear lattice size $\xi_{2\text{nd}}/L$ or the ratio of the partition functions for periodic and antiperiodic boundary conditions Z_a/Z_p are exploited. The comparison of results obtained from these different quantities allows us to estimate systematic errors that are caused by subleading corrections that are not explicitly taken into account in the fits.

The purpose of the present work is twofold. First, we improve the accuracy of the critical exponents of the three-dimensional XY universality class. These results provide a benchmark for future theoretical progress achieved by the conformal bootstrap or other methods. Second, we provide nonuniversal results, like, for example, inverse critical

temperatures, which are important groundwork for future studies. In particular, we intend to compute the structure constants using an approach similar to that in Ref. [28] for the Ising universality class. Furthermore, the improved $(N+1)$ -state clock model should be a good starting point to study the symmetry properties of the order parameter in the low-temperature phase.

The outline of the paper is the following: In Sec. II, we define the model and the observables that we measured. We summarize the theoretical basis of our finite-size scaling analysis in Sec. III. In Sec. IV, we discuss the Monte Carlo algorithm used in the simulations. In Sec. V, we analyze the data and present the results for the fixed point values of the dimensionless ratios, inverse critical temperatures, the correction exponent ω , and the critical exponents ν and η . Finally, we conclude and give an outlook. In the Appendix, we discuss the dependence of the critical temperature and other nonuniversal quantities on N and determine the RG exponent $\nu_{N=6}$ related to a Z_6 -invariant perturbation of the $O(2)$ invariant fixed point.

II. THE $(N+1)$ -STATE CLOCK MODEL

The model can be viewed as a generalization of the N -state clock model. The field \vec{s}_x at the site $x = (x_0, x_1, x_2)$, where $x_i \in 0, 1, 2, \dots, L_i - 1$, might assume one of the following values:

$$\vec{s}_x \in \{(0, 0), [\cos(2\pi m/N), \sin(2\pi m/N)]\}, \quad (3)$$

where $m \in \{1, \dots, N\}$. Compared with the N -state clock model, (0,0) is added as possible value of the field variable. In our program, we store the field variables by using labels $m = 0, 1, 2, \dots, N$. We assign

$$\vec{s}(0) = (0, 0) \quad (4)$$

and for $m > 0$

$$\vec{s}(m) = [\cos(2\pi m/N), \sin(2\pi m/N)]. \quad (5)$$

The reduced Hamiltonian is given by

$$\mathcal{H} = -\beta \sum_{\langle xy \rangle} \vec{s}_x \cdot \vec{s}_y - D \sum_x \vec{s}_x^2 - \vec{H} \sum_x \vec{s}_x, \quad (6)$$

where $\langle xy \rangle$ denotes a pair of nearest neighbor sites on the simple cubic lattice. We introduce the weight factor

$$w(\vec{s}_x) = \delta_{0, \vec{s}_x^2} + \frac{1}{N} \delta_{1, \vec{s}_x^2} = \delta_{0, m_x} + \frac{1}{N} \sum_{n=1}^N \delta_{n, m_x} \quad (7)$$

that gives equal weight to (0,0) and the collection of all values $|\vec{s}_x| = 1$. Now the partition function can be written as

$$Z = \sum_{\{\vec{s}\}} \prod_x w(\vec{s}_x) \exp(-\mathcal{H}), \quad (8)$$

where $\{\vec{s}\}$ denotes a configuration of the field. Note that in the limit $N \rightarrow \infty$, we recover the dynamically diluted XY (ddXY) model studied in Refs. [12,15]. The reduced Hamiltonian of the ddXY model has the same form as Eq. (6):

$$\mathcal{H}_{ddXY} = -\beta \sum_{\langle xy \rangle} \vec{\phi}_x \cdot \vec{\phi}_y - D \sum_x \vec{\phi}_x^2 - \vec{H} \sum_x \vec{\phi}_x, \quad (9)$$

where $\vec{\phi}_x$ is a vector with two real components. The partition function is given by

$$Z = \prod_x \left[\int d\mu(\phi_x) \right] \exp(-\mathcal{H}_{ddXY}), \quad (10)$$

with the local measure

$$d\mu(\phi_x) = d\phi_x^{(1)} d\phi_x^{(2)} \left[\delta(\phi_x^{(1)}) \delta(\phi_x^{(2)}) + \frac{1}{2\pi} \delta(1 - |\vec{\phi}_x|) \right]. \quad (11)$$

Note that the dynamically diluted XY model is a special case ($K = 0$) of the vectorialized Blume, Emery, and Griffiths (VBEG) model studied in Ref. [29].

A. Phase diagram of the dynamically diluted XY model

We expect that the phase diagram for $N \geq 5$ is essentially the same as that of the ddXY model. Therefore, we briefly recall the results obtained in Refs. [12,15]. In the limit $D \rightarrow \infty$, the XY model is recovered. There is a line of second-order phase transitions that ends at D_{tri} in a tricritical point. Following Ref. [15], based on mean-field calculations, $D_{\text{tri}} < 0$. Along the line of second-order phase transitions, there is a D^* , where leading corrections to scaling vanish. We refer to the ddXY model at $D \approx D^* = 1.06(2)$, Ref. [12], as the improved ddXY model. In Table II, we summarize results obtained for the inverse critical temperature β_c at various values of D . In Appendix B, we shall study the N dependence of β_c in detail.

B. Definitions of the measured quantities

The quantities studied are essentially the same as in Ref. [12]. For completeness, we list them below: The energy

TABLE II. Results for the inverse of the critical temperature β_c for the dynamically diluted XY model. These results are taken from Table II of Ref. [12].

| D | β_c |
|----------|------------------|
| 0.9 | 0.5764582(15)[9] |
| 1.02 | 0.5637963(2)[2] |
| 1.03 | 0.5627975(7)[7] |
| 1.2 | 0.5470376(17)[6] |
| ∞ | 0.4541652(5)[6] |

density is defined as

$$E = \frac{1}{V} \sum_{\langle xy \rangle} \vec{s}_x \cdot \vec{s}_y. \quad (12)$$

The magnetic susceptibility χ for a vanishing magnetization and the second-moment correlation length $\xi_{2\text{nd}}$ are defined as

$$\chi = \frac{1}{V} \left\langle \left(\sum_x \vec{s}_x \right)^2 \right\rangle \quad (13)$$

and

$$\xi_{2\text{nd}} = \sqrt{\frac{\chi/F - 1}{4 \sin^2 \pi/L}}, \quad (14)$$

where

$$F = \frac{1}{V} \left\langle \left| \sum_x \exp\left(i \frac{2\pi x_1}{L}\right) \vec{s}_x \right|^2 \right\rangle \quad (15)$$

is the Fourier transform of the correlation function at the lowest nonzero momentum. We consider several dimensionless quantities, which are also called phenomenological couplings. These quantities are, in the critical limit, invariant under RG transformations. We consider the Binder cumulant U_4 and its sixth-order generalization U_6 , defined as

$$U_{2j} = \frac{\langle (\bar{m}^2)^j \rangle}{\langle \bar{m}^2 \rangle^j}, \quad (16)$$

where $\bar{m} = \frac{1}{V} \sum_x \vec{s}_x$ is the magnetization of the system. We also consider the ratio $R_Z = Z_a/Z_p$ of the partition function Z_a of a system with antiperiodic boundary conditions in one of the three directions and the partition function Z_p of a system with periodic boundary conditions in all directions. Antiperiodic boundary conditions in the 0 direction are obtained by changing the sign of the term $\vec{s}_x \cdot \vec{s}_y$ of the Hamiltonian for links $\langle xy \rangle$ that connect the boundaries, i.e., for $x = (L, x_1, x_2)$ and $y = (0, x_1, x_2)$. In order to avoid microscopic effects at the boundary, we require that $-\vec{s}_x$ is in the same set of values as \vec{s}_x . Therefore, in the main part of the study, N is chosen to be even. In the following, we will refer to dimensionless ratios by R . Derivatives of dimensionless ratios with respect to the inverse temperature

$$S_R = \frac{\partial R}{\partial \beta} \quad (17)$$

are used to determine the critical exponent ν . In the following, these quantities are also denoted by slope of R .

For most of our analysis, we need the observables as a function of β in a certain neighborhood of the critical point. To this end, we simulate at β_s , which is a good approximation of β_c . In order to extrapolate in β , we compute the coefficients of the Taylor series in $\beta - \beta_s$ for all quantities listed above up to the third order. Note that a reweighting analysis is not possible, since, due to the large statistics, we performed a binning of the data already during the simulation.

III. FINITE-SIZE SCALING: THEORETICAL BACKGROUND

The account given below is similar to Sec. II B of Ref. [15]. The main purpose is to make the present paper self-contained. Our assumptions concerning subleading corrections differ from those of Ref. [15]. See Sec. III A below. Our starting point is the finite-size scaling behavior of the reduced free energy density, which is defined by

$$f(\beta, h, D, L) = -\frac{1}{V} \ln Z(\beta, h, D, L), \quad (18)$$

where Z is the partition function and $V = L^3$ is the number of lattice sites. Note that there is also a dependence on N that we suppress in the following to keep the notation tractable.

The reduced free energy density can be written in terms of the analytic functions $\mathcal{F}_{\text{sing}}$ and g ; see, for example, Eq. (2.14) of Ref. [4],

$$f(\beta, h, D, L) = L^{-d} \mathcal{F}_{\text{sing}}(L^{y_t} u_t, L^{y_h} u_h, \{u_i L^{y_i}\}) + g(\beta, h, D), \quad (19)$$

where d is the dimension of the system. Note that $\mathcal{F}_{\text{sing}}$ is a universal function, which, however, depends on the global geometry of the system, for example, on aspect ratios L_i/L_j , where $i \neq j$ are the directions on the lattice or on the type of boundary conditions. Here, we consider periodic and antiperiodic boundary conditions that do not generate boundary contributions, like Dirichlet boundary conditions, for example. The analytic background $g(\beta, h, D)$ does not depend on these global properties. u_t and u_h are the temperature-like and external-field-like scaling fields with the RG exponents y_t and y_h , respectively. These are the only relevant RG-exponents: $y_t > 0$ and $y_h > 0$. In addition, there are irrelevant RG exponents $y_i < 0$. Below we summarize results on irrelevant RG exponents given in the literature. Following, for example, Ref. [4], Sec. 1.5.7, the nonlinear scaling fields can be written as

$$u_t = g_{01}(D) t + g_{11}(D) t^2 + g_{12}(D) h^2 + O(t^3, th^2, h^4), \quad (20)$$

$$u_h = g_{02}(D) h[1 + g_{12}(D) t + g_{22}(D) h^2 + O(t^2, th^2, h^4)], \quad (21)$$

where we define the reduced temperature as $t = \beta_c(D) - \beta$. Note that $\beta_c(D)$ and the coefficients $g_{ij}(D)$ depend on N . In Appendix B, we show, however, that there is a fast convergence as $N \rightarrow \infty$. The external field is written as $\vec{H} = h\vec{H}_0$, where \vec{H}_0 is a two-component unit vector. We have introduced $g_{01}(D)$ and $g_{02}(D)$ to get the same function $\mathcal{F}_{\text{sing}}$ for all values of D on the critical line. The scaling field of the leading correction is

$$u_3 = g_{13}(D) + g_{23}(D) t + g_{33}(D) h^2 + O(t^2, th^2, h^4). \quad (22)$$

The improved model is characterized by $g_{13}(D^*) = 0$. Note that in general $g_{23}(D^*) \neq 0$ and $g_{33}(D^*) \neq 0$. Also note that

D^* depends on N , since $g_{13}(D)$ depends on N . For numerical results, see Appendix B 3.

A. Irrelevant RG exponents

Let us briefly summarize results on RG exponents for the three-dimensional XY -universality class given in the literature. Various methods give, at least qualitatively, a consistent picture for the relevant RG eigenvalues y_t and y_h and the leading irrelevant RG eigenvalue y_3 . Using scaling relations (see, for example, Ref. [4], Secs. 1.3 and 1.5.1), these are related with the critical exponents given in Table I as

$$y_t = 1/\nu, \quad y_h = \frac{d+2-\eta}{2}, \quad y_3 = -\omega. \quad (23)$$

Scaling fields can be classified according to the symmetry properties of the operators associated to them. The simple cubic lattice breaks the Galilean symmetries of continuous space. The leading correction associated has the RG exponent $y_{NR} = -2.02(1)$ [12,15,30]. Note that in the case of the three-dimensional Ising universality class, $y_{NR} = -2.0208(12)$ given in Table I of Ref. [31] is in reasonable agreement with $y_{NR} = -2.022665(28)$ that follows from $\Delta = 5.022665(28)$ for angular momentum $l = 4$ given in Table 2 of Ref. [16].

Results for subleading corrections are provided by different incarnations of the renormalization group. Newman and Riedel [32] studied the fixed point of the $O(N)$ invariant ϕ^4 theory in three dimensions using the scaling field method. They predict by using the scaling field method subleading corrections with $y_{421} = -1.77(7)$ and $y_{422} = -1.79(7)$, which are nearly degenerate. For the meaning of the indices, see Ref. [32]. In Refs. [12,15] the analysis of the data is based on this result. Note that Newman and Riedel find $y_{422} = -1.67(11)$ in the case of the Ising universality class, which is not confirmed by the conformal bootstrap method. Instead, $y'' = -3.8956(43)$ is found; see the estimate related to the operator ϵ'' given in Table 2 of Ref. [16]. In fact, the estimates for subleading correction exponents obtained by the functional renormalization group (FRG) (see, for example, Ref. [33]) are in better agreement with those of the conformal bootstrap method. In Table 3 of Ref. [34], results for correction exponents for a large range of N , where N refers to the $O(N)$ symmetry of the theory, are given. The qualitative picture is the same for all N and the numerical values change slowly with varying N . Therefore, we regard it as plausible that $-3.5 \gtrsim y'' \gtrsim -4$ for the three-dimensional XY universality class. Note that skipping corrections $\propto L^{-1.77}$ in the analysis of our data virtually does not change the central values of the final results. Estimates of the error are reduced by a factor of $\approx 2/3$.

Finally, let us recall the results for the RG exponent associated with a Z_N invariant perturbation. The authors of Ref. [5] obtain $-y_N = 0.128(6), 1.265(6), 2.509(7), 3.841(8), 5.278(9), 6.796(9), 8.399(10), 10.077(11),$ and $11.825(12)$ for $N = 4, 5, 6, \dots, 12$, respectively. In the main part of our study, we have simulated the $(N+1)$ -state clock model for $N = 8$. For this value of N , we can ignore deviations from $O(2)$ invariance in the finite-size scaling analysis of our

data as can be clearly seen from the analysis presented in Appendix B 4.

B. The magnetic susceptibility and the energy density

The magnetic susceptibility at $h = 0$ for vanishing magnetization is

$$\chi = -\frac{2}{V} \frac{\partial^2 f}{\partial h^2} \Big|_{h=0} = \frac{1}{V} \left\langle \left(\sum_x \bar{s}_x \right)^2 \right\rangle. \quad (24)$$

Note that we have introduced a factor of 2 here to stay consistent with the definition (13) above.

Let us define $\tilde{u}_t = u_t L^{y_t}$, $\tilde{u}_h = u_h L^{y_h}$, and $\tilde{u}_i = u_i L^{y_i}$. Now let us compute the second partial derivative of f with respect to h at $h = 0$:

$$\frac{\partial^2 f}{\partial h^2} \Big|_{h=0} = L^{-d} \frac{\partial^2 \mathcal{F}_{\text{sing}}}{\partial h^2} \Big|_{h=0} + \frac{\partial^2 g}{\partial h^2} \Big|_{h=0}, \quad (25)$$

where

$$\begin{aligned} L^{-d} \frac{\partial^2 \mathcal{F}_{\text{sing}}}{\partial h^2} \Big|_{h=0} &= \frac{\partial \mathcal{F}_{\text{sing}}}{\partial \tilde{u}_t} \Big|_{h=0} 2 (g_{12}(D) + \dots) L^{y_t-d} \\ &+ \frac{\partial^2 \mathcal{F}_{\text{sing}}}{\partial \tilde{u}_h^2} \Big|_{h=0} (g_{02}(D) [1 + g_{12}(D)t + \dots])^2 L^{2y_h-d} \\ &+ \dots \end{aligned} \quad (26)$$

There are also contributions stemming from partial derivatives with respect to \tilde{u}_i . However, these are related with correction exponents $\epsilon > 4$ and therefore play little role in the analysis of the data.

It remains to Taylor expand $\frac{\partial^2 \mathcal{F}_{\text{sing}}}{\partial \tilde{u}_h^2} \Big|_{h=0}$ and $\frac{\partial \mathcal{F}_{\text{sing}}}{\partial \tilde{u}_t} \Big|_{h=0}$ in \tilde{u}_i . We arrive at corrections that are proportional to L^{y_3} , L^{2y_3} , L^{3y_3} , \dots , $L^{y_{NR}}$, $L^{y_{NR}+y_3}$, \dots , $L^{y''}$, \dots . Note that for an improved model, all terms with y_3 in the exponent have a vanishing amplitude, since $u_3 = 0$. For an improved model, at the critical point we get

$$\chi_{h=0, t=0, D=D^*} = aL^{2y_h-d} [1 + c_{NR}L^{y_{NR}} + c''L^{y''} + c_t L^{y_t-2y_h} + \dots] + b. \quad (27)$$

Note that $2y_h - d = 2 - \eta$. The analytic background b can be viewed as a correction with the RG exponent $y_b = \eta - 2 \approx -1.962$, which is close to $y_{NR} = -2.02(1)$. Also, the value of $y_t - 2y_h \approx -3.473$ is close to that of y'' .

The energy density, Eq. (12), is given by the first derivative of the free energy with respect to t . At the critical point, we get

$$\begin{aligned} \frac{\partial f}{\partial t} \Big|_{t=0, h=0} &= \frac{\partial \mathcal{F}_{\text{sing}}}{\partial \tilde{u}_t} \Big|_{t=0, h=0} g_{01}(D) L^{y_t-d} + \frac{\partial \mathcal{F}_{\text{sing}}}{\partial \tilde{u}_3} \Big|_{t=0, h=0} \\ &\times g_{23}(D) L^{y_t-d} + \frac{\partial g}{\partial t} \Big|_{t=0, h=0}. \end{aligned} \quad (28)$$

It remains to Taylor expand $\frac{\partial \mathcal{F}_{\text{sing}}}{\partial \tilde{u}_t} \Big|_{t=0, h=0}$ in \tilde{u}_i . We arrive at

$$E = E_0 + aL^{y_t-d} (1 + c_{NR}L^{y_{NR}} + c_3 L^{y_3-y_t} + c''L^{y''} + \dots) \quad (29)$$

for an improved model at the critical point. Note that $y_3 - y_t \approx -2.278$ is only slightly smaller than y_{NR} .

C. Phenomenological couplings

Cornerstones of our analysis are dimensionless quantities which are also called phenomenological couplings. In the following, we shall denote them by R , since in our case they are ratios. The first quantity that we consider is the ratio of partition functions. We get

$$\ln \frac{Z_a}{Z_p} = V(f_p - f_a) = \mathcal{F}_{p,\text{sing}} - \mathcal{F}_{a,\text{sing}}, \quad (30)$$

since the analytic background exactly cancels. Hence,

$$\frac{Z_a}{Z_p} = R_Z(L^{y_t} u_t, L^{y_h} u_h, \{L^{y_j} u_j\}). \quad (31)$$

In addition we study the cumulants

$$U_{2j} = \frac{\langle m^{2j} \rangle}{\langle m^2 \rangle^j} \quad (32)$$

for $j = 2$ and 3 . Here, we can build on the result obtained above for the magnetic susceptibility. Also, $\langle m^{2j} \rangle$ can be computed from partial derivatives of the free energy density with respect to the external field h . The dominant contributions stem from the derivatives of the singular part of the free energy with respect to \tilde{u}_h and even derivatives of the singular part of the free energy with respect to \tilde{u}_t . Hence,

$$\begin{aligned} U_{2j} &= R_U(L^{y_t} u_t, L^{y_h} u_h, \{L^{y_i} u_i\}) + aL^{-2y_h+d} \\ &+ bL^{-2y_h+y_t} + \dots \end{aligned} \quad (33)$$

In the case of the second moment correlation length $\xi_{2\text{nd}}$ divided by the linear lattice size L , we also expect corrections that go back to the magnetic susceptibility. In addition, there is a correction $\propto L^{-2}$ due to the construction of $\xi_{2\text{nd}}$.

Taking the derivative of a phenomenological coupling with respect to the reduced temperature t , we get

$$\begin{aligned} \frac{\partial R}{\partial t} \Big|_{h=0} &= \frac{\partial R}{\partial \tilde{u}_t} \Big|_{h=0} [g_{01}(D) + g_{11}(D)t + \dots] L^{y_t} + \frac{\partial R}{\partial \tilde{u}_3} \Big|_{h=0} \\ &\times g_{23}(D) L^{y_3} + \dots \end{aligned} \quad (34)$$

At the critical point of an improved model,

$$\begin{aligned} \frac{\partial R}{\partial t} \Big|_{t=0, h=0, D=D^*} &= aL^{y_t} (1 + cL^{y_{NR}} + \dots + d g_{23}L^{-y_t+y_3} + \dots), \end{aligned} \quad (35)$$

where we performed a Taylor expansion of $\frac{\partial R}{\partial \tilde{u}_t}$ and $\frac{\partial R}{\partial \tilde{u}_3}$ with respect to $\{\tilde{u}_i\}$.

D. Fixing the value of R

In the analysis of our data, we consider certain quantities at a fixed value R_f of a dimensionless quantity. This means that for each lattice size L , we compute $\beta_f(D, L)$ defined by

$$R(\beta_f(D, L), D, L) = R_f. \quad (36)$$

Note that we have skipped the argument h , since $h = 0$ throughout. Making use of Eq. (31), we get

$$R(\beta_f, D, L) = R^* + a(D)(\beta_c(D) - \beta)L^{y_t} + \dots + c(D)L^{y_3} + \dots \quad (37)$$

for $R_f \approx R^*$, where R^* is the fixed point value of R . Hence,

$$\beta_f(D, L) = \beta_c(D) - a(D)^{-1}(R^* - R_f)L^{-y_t} + \dots + a(D)^{-1}c(D)L^{y_3 - y_t} + a(D)^{-1}d(D)L^{y_{NR} - y_t} + \dots \quad (38)$$

Note that $c(D^*) = 0$. First, we consider a phenomenological coupling R_2 at a fixed value $R_{1,f}$ of an other phenomenological coupling R_1 . One gets

$$R_2(R_{1,f}, D, L) = r_2(R_{1,f}, \{\tilde{u}_i\}) + c(R_{1,f}, D)L^{y_3 - y_t} + \dots + d(D)L^{2y_3 - y_t} + \dots, \quad (39)$$

where $c(R_1^*, D) = 0$. Note that the corrections are due to the fact that the u_i depend on t ; see Eq. (22).

We also compute the magnetic susceptibility and the slope of phenomenological couplings at R_f . Plugging Eq. (38) into Eqs. (26), (34), we see that compared with Eqs. (27) and (35) additional correction terms proportional to $(R_f - R^*)L^{-y_t}$, $(D - D^*)L^{-y_t + y_3}$ and $L^{-y_t + y_{NR}}$ appear. Therefore, it is favorable to take $R_f \approx R^*$. In the numerical analysis, one should vary R_f to check the effect of a possible deviation from R^* .

IV. THE ALGORITHM

As in previous studies, for example, Refs. [12,15], we have implemented a hybrid of local Metropolis updates, the single cluster update [35], and the wall cluster update [21]. Now let us discuss in detail these components of the algorithm and their implementation.

A. Local Metropolis algorithm

As usual, in the elementary step of the local update, the variable at a single site is changed, while all other variables are kept fixed. Using these elementary updates, we go through the lattice in typewriter fashion. Going through the lattice once is called a sweep. We use two different ways to generate the proposal for the local Metropolis update. In both cases, the proposal $\{\vec{s}\}'$ is accepted with the probability

$$P_{acc} = \min[1, \exp(-\Delta H)], \quad (40)$$

where

$$\Delta H = H(\{\vec{s}\}') - H(\{\vec{s}\}). \quad (41)$$

The weight, Eq. (7), is taken into account by the probabilities used to generate the proposal. The first choice is given by the following probabilities: If $\vec{s}_x = (0, 0)$, we take with equal probability one of the N values with $|\vec{s}'_x| = 1$ as proposal. Else, for $|\vec{s}_x| = 1$, we always take $\vec{s}'_x = (0, 0)$ as the proposal.

For an efficient implementation, one should avoid computing $\exp(\cdot)$ for each update step. Instead, we should store possible results in a table before the actual simulation is started.

The sum of all nearest neighbor spins can take a number of possible values that is too large to store $\exp(-\Delta H)$ efficiently. Therefore, we tabulate instead the contribution to the Boltzmann factor by pairs

$$B(m, n) = \exp[\beta \vec{s}(m) \cdot \vec{s}(n)] \quad (42)$$

and its inverse $B^{-1}(m, n)$. Furthermore, $\exp(-D)$ and $\exp(D)$ are computed once and are then stored. Then, for $m_x = 0$, where x is the site to be updated, we get

$$\exp(-\Delta H) = \exp(D) \prod_{y.nn.x} B(m'_x, m_y), \quad (43)$$

where the product runs over all nearest neighbors (nn) of x . Note that $B(0, n) = 1$ for all values of n . For $m_x > 0$, we get

$$\exp(-\Delta H) = \exp(-D) \prod_{y.nn.x} B^{-1}(m_x, m_y). \quad (44)$$

Since we were not able to prove the ergodicity of this algorithm, we used in addition a second choice of the proposal. It is generated independently of the old value of the variable. With probability $1/2$, we take $\vec{s}'_x = (0, 0)$ and with equal probabilities $1/(2N)$ one of the remaining values is chosen. Here

$$\exp(-\Delta H) = \exp(-D[\vec{s}_x^2 - \vec{s}'_x'^2]) \times \prod_{y.nn.x} [B^{-1}(m_x, m_y)B(m'_x, m_y)]. \quad (45)$$

This update takes more computer processing time than the first. However, ergodicity is obvious.

B. Cluster algorithms

Cluster algorithms can be applied without major modifications compared with the ddXY model. We just have to note that the reflection has to be chosen such that the field variables remain in the allowed set of values. A reflection is given by

$$\vec{s}' = \vec{s} - 2(\vec{r} \cdot \vec{s})\vec{r}, \quad (46)$$

where

$$\vec{r} = [\cos(\pi m/N), \sin(\pi m/N)] \quad (47)$$

with $m = 0, 1, 2, \dots, N-1$. The cluster update is characterized by the delete probability [15,35]

$$p_d(\vec{s}_x, \vec{s}_y) = \min[1, \exp(-2\beta[\vec{r} \cdot \vec{s}_x][\vec{r} \cdot \vec{s}_y])]. \quad (48)$$

The values of p_d are tabulated before the actual simulation is started. For a discussion of the single cluster [35] and the wall cluster update [21] used for the simulation of the ddXY model, see Refs. [12,15].

C. The implementation

Our simulations are organized in a similar fashion as in Refs. [12,15]. Since we could not store the results of all measurements on hard disk, we performed a binning of the data during the simulation.

During the study, we varied the precise composition of the update cycle. In most of the simulations, the following cycle,

given by a C code, is used:

```

for(i=0;i<N_bin;i{++)
{
  Metropolis_2();
  for(k=0;k<6;k{++)
  {
    Metropolis_1();
    for(j=0;j<L;j{++)  single_cluster();
    Metropolis_1();
    wall_cluster(direction=k%3);
    measurements();
  }
}

```

Here `Metropolis_1()` and `Metropolis_2()` are sweeps, using the first and second types of the Metropolis update discussed in Sec. IV A. The single cluster update is given by `single_cluster()` and `wall_cluster(direction=k%3)` is a wall cluster update for one of the three spacial directions. The plane is perpendicular to the k axis. The position of the plane is randomly chosen in $\{0, 1, 2, \dots, L-1\}$. In order to compute Z_a/Z_p , we need two subsequent wall cluster updates, where the two reflection axes are perpendicular. The first axis is chosen randomly among the N possible directions.

We did run our program on standard x86 CPUs. For lack of human time, we made no attempt to implement our program on a graphics processing unit (GPU). For cluster algorithms on GPUs, see, for example, Refs. [36,37].

Let us briefly comment on the CPU time required by the different components of the update cycle. We performed the simulations on various PCs and servers at the institute of theoretical physics. Here, we quote numbers for a single core of an Intel Xeon CPU E3-1225 v3 running at 3.20 GHz. We implemented the code in standard C and used the SIMD-oriented fast Mersenne twister algorithm [38] as random number generator.

Our Metropolis update type 1 requires 1.2×10^{-8} s per site. In the case of the single cluster update, about 3.8×10^{-8} s per site are needed. Note that the random number generator requires for one sequential access about 3×10^{-9} s. Compared with our program for the ddXY model, these updates are faster by roughly a factor of 3.

Plots were generated by using the MATPLOTLIB library [39]. The least square fits were performed by using the function `curve_fit()` contained in the SCIPY library [40] with the default Levenberg-Marquardt algorithm [41–43]. The function `curve_fit()` acts as a wrapper to functions contained in the MINPACK library [44].

V. THE SIMULATIONS AND THE ANALYSIS OF THE DATA

We simulated the model for $N = 8$ at various values of D , close to the inverse critical temperature $\beta_c(D)$. Most CPU time is spent on simulations for $D = 1.02, 1.05$, and 1.07 which are close to D^* . We simulated linear lattice sizes up to $L = 512$, where the statistics is decreasing with increasing L . In Fig. 1, we plot the number of measurements times the volume L^3 as a function of the linear lattice size L for $D = 1.05$ and 1.07 . In the case of $D = 1.02$, the statistics

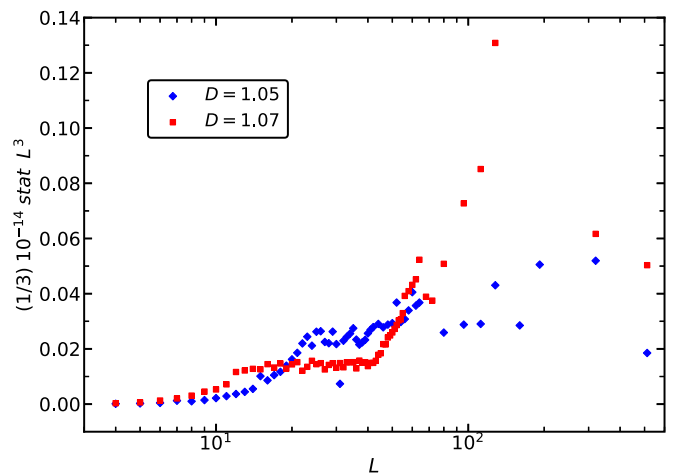


FIG. 1. We plot the number of measurements times the volume L^3 as a function of the linear lattice size L for $N = 8$ at $D = 1.05$ and $D = 1.07$.

is similar but we have simulated at fewer lattice sizes in the range $L = 20$ up to 80 . In addition, we simulated at $D = -0.7, -0.5, 0, 0.45, 0.9, 1.24$, and ∞ . In these cases, we considered linear lattice sizes up to $L = 64, 64, 72, 72, 48, 48$, and 72 , respectively. The main purpose of these simulations is to determine the correction exponent ω . A few simulations at $D = -0.85, -0.86$, and -0.87 are performed to obtain a rough estimate of the tricritical point.

Our simulations were performed on various personal computers and servers. In total, these simulations took the equivalent of about 50 years of CPU time on a single core of an Intel Xeon CPU E3-1225 v3 running at 3.20 GHz. Note that the study was not systematically designed at the start but grew with time, also depending on the availability of CPU time.

Let us briefly comment on the assessment of the error of the final estimates for critical exponents and other quantities of interest. In the ansätze, we can take into account only a small number of correction terms. This inevitably leads to systematic errors caused by corrections to scaling that are not explicitly taken into account. A large $\chi^2/\text{d.o.f.}$ indicates that the ansatz is not adequate to represent the data. However, when dealing with an ansatz that does not fully represent the underlying function, a small $\chi^2/\text{d.o.f.}$ and a corresponding acceptable goodness of the fit say very little on the deviation of the fit parameters from their true values. In order to get some handle on systematic errors caused by corrections to scaling that are not taken into account in the ansatz, we either consider a number of different quantities or ansätze with a different number of correction terms. The final estimate and its error bar are chosen such that these different estimates are covered. The actual choice, which fits and minimal lattice sizes are taken into account, is at least partially an *ad hoc* decision. To allow the reader an own assessment, the direct outcome of fits is given in figures. We made no effort to give a separate estimate of the statistical and systematic error, since they are interwoven in our assessment.

The analysis of the data is organized in the following way: First, we perform joint fits of our data for the dimensionless quantities R for $D = 1.02, 1.05$, and 1.07 . The results are the fixed point values R^* and estimates of the inverse critical

temperatures. Next, we include values of D with a larger amplitude of the leading correction to determine the exponent ω . To this end, we analyze the cumulants U_4 and U_6 at a fixed values of either Z_a/Z_p or ξ_{2nd}/L . Then we determine D^* focusing again on $D = 1.02, 1.05, \text{ and } 1.07$. It follows a rough localization of the tricritical point D^* . In the final step of the analysis, we determine the critical exponents ν and η . To this end, we analyze the finite-size scaling behavior, the slopes of dimensionless quantities R , the energy density, and the magnetic susceptibility.

A. The critical coupling β_c and the fixed point values of dimensionless ratios R^*

First, we determined the critical coupling $\beta_c(D)$ and the fixed point values R^* of the dimensionless quantities that we have computed. To this end, we analyzed our data at $D = 1.02, 1.05, \text{ and } 1.07$, which are close to D^* .

Motivated by Eqs. (31) and (33), we have fitted our data with four different ansätze:

$$R(L, D, \beta_c(D)) = R^*, \quad (49)$$

$$R(L, D, \beta_c(D)) = R^* + b(D)L^{-\epsilon_1}, \quad (50)$$

$$R(L, D, \beta_c(D)) = R^* + b(D)L^{-\epsilon_1} + c(D)L^{-\epsilon_2}, \quad (51)$$

$$R(L, D, \beta_c(D)) = R^* + b(D)L^{-\epsilon_1} + c(D)L^{-\epsilon_2} + d(D)L^{-\epsilon_3}. \quad (52)$$

We need the phenomenological couplings R as a function of the inverse temperature. To this end, we have used the Taylor series around the value β_s of the inverse temperature used in the simulation. We have checked that β_c and β_s are sufficiently close to avoid significant truncation effects. This way, for example, Eq. (50) becomes

$$R(L, \beta_s) = R^* - c_1(L, \beta_s)(\beta_c - \beta_s) - \frac{c_2(L, \beta_s)}{2!}(\beta_c - \beta_s)^2 - \frac{c_3(L, \beta_s)}{3!}(\beta_c - \beta_s)^3, \quad (53)$$

where R^* and β_c are the two parameters of the fit.

It turned out that fits with the ansatz (50) are not very useful, since the amplitude of leading corrections is small for the values of D considered here. Therefore, we shall not discuss the results of these fits in the following. Furthermore, we did not consider ansätze with $\epsilon_2 = 2\omega$ here, since the amplitude of such corrections should be very small. This will be verified below in Sec. VB. In the case of Z_a/Z_p , we have used in Eq. (51) the choices $\epsilon_1 = 0.79$ and $\epsilon_2 = 2.02$. In Eq. (52), we used in addition either $\epsilon_3 = 3.5$ or $\epsilon_3 = 4$. Note that below, in Sec. VB, we shall find $\omega = 0.789(4)$, Eq. (58).

We performed a preliminary analysis using different parametrizations and choices of data sets. Based on this analysis, we decided to extract the final results in the following way: We performed joint fits for the three values $D = 1.02, 1.05, \text{ and } 1.07$, where we parametrize the amplitude of the leading correction as

$$b(D) = b_s(D - D^*) \quad (54)$$

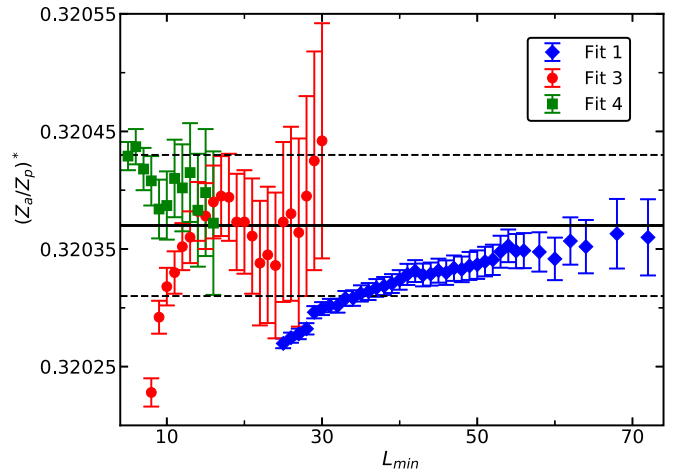


FIG. 2. We give the results for $(Z_a/Z_p)^*$ fitting with the ansätze (49), (51), and (52) with $\epsilon_3 = 4$, corresponding to fits 1, 3, and 4 in the legend of the figure, as a function of the minimal lattice size L_{\min} that is included in the fit. Data for $D = 1.02, 1.05, \text{ and } 1.07$ are jointly fitted. The solid line gives our final estimate and the dashed ones the corresponding error.

and the amplitudes of higher corrections, $c(D)$ and $d(D)$ are assumed to be the same for all three values of D .

First, we analyzed the data for the ratio of partition functions Z_a/Z_p . In Fig. 2, we plot results for $(Z_a/Z_p)^*$ of fits using the ansätze (49), (51), and (52). We give only data points with $\chi^2/\text{d.o.f.} < 4$. In the case of ansatz (49), we see that $\chi^2/\text{d.o.f.}$ decreases rapidly with increasing L_{\min} , where L_{\min} is the minimal lattice size that is included into the fit. For $L_{\min} = 33$, $\chi^2/\text{d.o.f.} = 1.012$ is reached. For ansatz (51), we find $\chi^2/\text{d.o.f.} = 0.986$ already for $L_{\min} = 9$. As amplitude of the correction $\propto L^{-2.02}$, we find $c \approx -0.07$. For ansatz (52) with $\epsilon_3 = 4$, we find $\chi^2/\text{d.o.f.} = 0.972$ for $L_{\min} = 5$. The amplitude of the correction $\propto L^{-4}$ is $d \approx -1.6$. Consistently with ansatz (51), we find $c \approx -0.06$. Using $\epsilon_3 = 3.5$ instead, we get $\chi^2/\text{d.o.f.} = 1.135$ for $L_{\min} = 5$ and $\chi^2/\text{d.o.f.} = 0.889$ for $L_{\min} = 7$. For $L_{\min} = 7$, we get $d = -0.85(4)$ and $c = -0.028(5)$. The fact that the amplitude of the correction $\propto L^{-\epsilon_3}$ is much larger than that of $\propto L^{-2.02}$ is surprising.

Our final estimate

$$(Z_a/Z_p)^* = 0.32037(6) \quad (55)$$

is taken such that it is consistent with the results of the three different ansätze. Note that we also varied the values of ϵ_1 and ϵ_2 within the range of the expected error bars. The results of the fits change little. In a similar way, we arrive at the estimates for D^* and β_c at $D = 1.02, 1.05, \text{ and } 1.07$. These estimates are given in Table III.

Next, we analyzed the data for the ratio ξ_{2nd}/L and the cumulants U_4 and U_6 in a similar way, taking into account that also corrections $\propto L^{\eta-2}$ might be present. The final results are summarized in Table III.

The estimates for R^* can be compared with $(Z_a/Z_p)^* = 0.3203(1)$ [3], $(\xi_{2nd}/L)^* = 0.5924(1)$ [3], $U_4^* = 1.2431(1)$ [1], and $U_6^* = 1.7509(2)$ [7] given in Table I of Ref. [12]. These results were obtained by analyzing data obtained for the two-component ϕ^4 and the ddXY model on the simple

TABLE III. In the first column, the phenomenological coupling is specified. In the second column, we give the corresponding estimates of the fixed point values R^* . In the third column, we give the estimates of D^* , where leading corrections to scaling vanish. In the following columns, the estimates of the inverse critical temperature β_c for $D = 1.02, 1.05$, and 1.07 are given. These estimates are based on joint fits of our data for $D = 1.02, 1.05$, and 1.07 , as discussed in the text. In the last row, we give our final estimates of β_c .

| R | R^* | D^* | $\beta_c(1.02)$ | $\beta_c(1.05)$ | $\beta_c(1.07)$ |
|---------------|-------------|-----------|-----------------|-----------------|-----------------|
| Z_a/Z_p | 0.32037(6) | 1.065(35) | 0.56379620(8) | 0.56082390(7) | 0.55888342(7) |
| ξ_{2nd}/L | 0.59238(7) | 1.075(25) | 0.56379622(9) | 0.56082391(8) | 0.55888342(8) |
| U_4 | 1.24296(8) | 1.054(10) | 0.56379626(8) | 0.56082386(8) | 0.55888335(10) |
| U_6 | 1.75040(25) | 1.054(10) | 0.56379626(8) | 0.56082386(8) | 0.55888335(10) |
| | | | 0.56379622(10) | 0.56082390(10) | 0.55888340(10) |

cubic lattice. In Ref. [12], the authors tried to distinguish between statistical () and systematical [] error. We find a nice agreement of the estimates, giving support to the hypothesis that the improved $(8 + 1)$ -state clock model shares the three-dimensional XY universality class.

The estimates of D^* and β_c obtained from U_4 and U_6 are the same up to the digits given here. In contrast, the differences with the estimates obtained from Z_a/Z_p and ξ_{2nd}/L are of similar size as the statistical errors. These differences are likely due to subleading corrections that are not taken into account in the ansätze. We find that the error of D^* obtained from Z_a/Z_p or ξ_{2nd}/L is larger than that of D^* obtained from U_4 or U_6 . Below in Sec. VB 2, we give our final estimate of D^* . In the last row of Table III, we give our final estimates of β_c , which are mainly based on the analysis of Z_a/Z_p and ξ_{2nd}/L . The error bars are chosen such that the estimates obtained from Z_a/Z_p and ξ_{2nd}/L , including their error bars are covered. For the inverse critical temperature at the remaining values of D , see Appendix A.

B. Corrections to scaling

In this section, we focus on corrections to scaling. To this end, it is useful to consider the cumulants U_4 and U_6 at a fixed value of Z_a/Z_p or ξ_{2nd}/L [21]. In particular, we take $Z_a/Z_p = 0.32037$ and $\xi_{2nd}/L = 0.59238$, which are our estimates of the fixed point values of these quantities. This means that U_4 and U_6 are taken at β_f , where β_f is chosen such that either $Z_a/Z_p = 0.32037$ or $\xi_{2nd}/L = 0.59238$. In the following, we denote a cumulant at a fixed value of Z_a/Z_p or ξ_{2nd}/L by \bar{U} . Taylor expanding Eq. (39), we get

$$\bar{U} = \bar{U}^* + b(D)L^{-\omega} + cb^2(D)L^{-2\omega} + \dots + d(D)L^{-\omega_2} + \dots + [f(R_f - R^*) + g(D - D^*)]L^{-1/\nu - \omega} + \dots, \quad (56)$$

where R denotes either Z_a/Z_p or ξ_{2nd}/L . Note that here f and g are coefficients and not functions.

In Fig. 3, as a first step of the analysis, we plot U_4 at $Z_a/Z_p = 0.32037$ for $D = 0.45, 0.9, 1.05, 1.24$, and ∞ . We have omitted $D = 1.02$ and 1.07 to keep the figure readable. For $D = 1.05$, we see very little dependence of \bar{U}_4 on L , which confirms that $D = 1.05$ is close to D^* . For $D = \infty$, we find that \bar{U}_4 is increasing with increasing lattice size. It is approaching the curve for $D = 1.05$. For $D = 0.45$, we see that \bar{U}_4 is decreasing and the amplitude of the corrections is roughly equal to that at $D = \infty$, but with the opposite sign. Next, in Fig. 4, we plot U_4 at $Z_a/Z_p = 0.32037$ for $D = -0.7$,

$-0.5, 0$, and 0.45 . Going to smaller values of D , much larger amplitudes of the leading correction can be obtained than for $D \rightarrow \infty$. Still for $D = -0.7$, where the amplitude of the corrections is the largest, the fixed point value is approached as the lattice size increases. This indicates that $D = -0.7$ is on the line of second-order phase transitions. Below, we shall study the tricritical point, which is located at a smaller value of D .

In the following, we determine the exponent of the leading corrections ω and D^* , the value of D , where the amplitudes of leading corrections vanish.

1. The correction exponent ω

We performed joints fits of our data for $D = -0.7, -0.5, 0.0, 0.45, 0.9, 1.02, 1.05, 1.07, 1.24$, and ∞ . We used the ansatz

$$\bar{U} = \bar{U}^* + \sum_{i=1}^{i_{\max}} c_i [b(D)L^{-\omega}]^i + dL^{-\epsilon}. \quad (57)$$

In order to avoid ambiguity, we set $c_1 = 1$. In most of our fits, we used $\epsilon = 2$. Furthermore, it is assumed that d does not depend on D . At least for corrections due to the breaking of the rotational invariance this should be a good approximation. As a check, we also performed fits without the term $dL^{-\epsilon}$. Since our final results are taken from fits with $L_{\min} \geq 16$, the

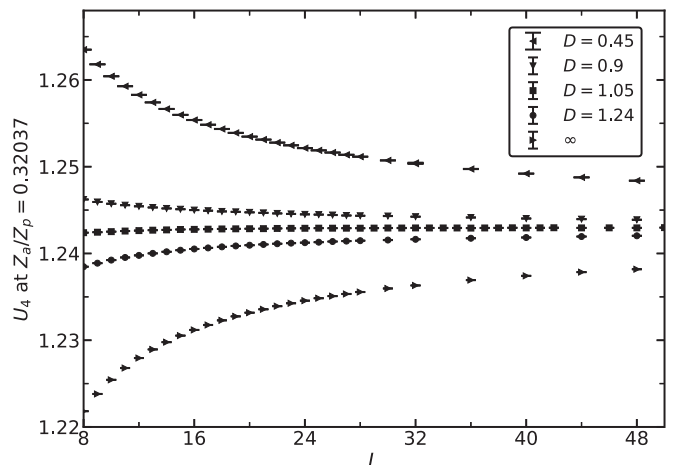


FIG. 3. We plot U_4 at $Z_a/Z_p = 0.32037$ for $N = 8$ at $D = 0.45, 0.9, 1.05, 1.24$, and ∞ as a function of the linear lattice size L .

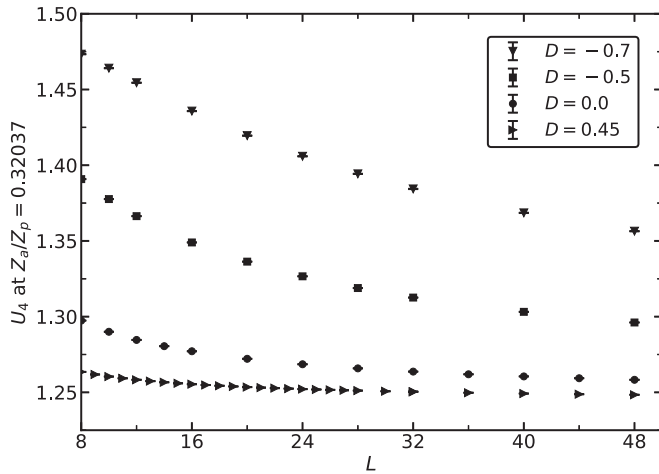


FIG. 4. We plot U_4 at $Z_a/Z_p = 0.32037$ for $N = 8$ at $D = 0.45, 0.0, -0.5,$ and -0.7 as a function of the linear lattice size L .

term $dL^{-\epsilon}$ has only a small effect. The free parameters of our fits are $\bar{U}^*, b(D), c_i, \omega,$ and d .

First, we fitted all data for all values of D listed above that satisfy $L \geq L_{\min}$. Here, we performed fits with $i_{\max} = 2, 3, 4, 5, 6$. It turns out that the results for \bar{U}_4^*, \bar{U}_6^* , and ω depend on i_{\max} . Let us focus the discussion on ω , which is the most important quantity.

In Fig. 5, we plot the results obtained from fits with $i_{\max} = 3, 4, 5,$ and 6 of U_4 at $Z_a/Z_p = 0.32037$. We see that the estimates of ω are increasing with increasing i_{\max} . For $i_{\max} = 5$ and 6 , the values saturate. In the plot, we give only results that correspond to $\chi^2/\text{d.o.f.} < 4$. With increasing L_{\min} the $\chi^2/\text{d.o.f.}$ rapidly converge to $\chi^2/\text{d.o.f.} \approx 1$. As our intermediate result of this set of fits, we take $\omega = 0.7886(11)$ from

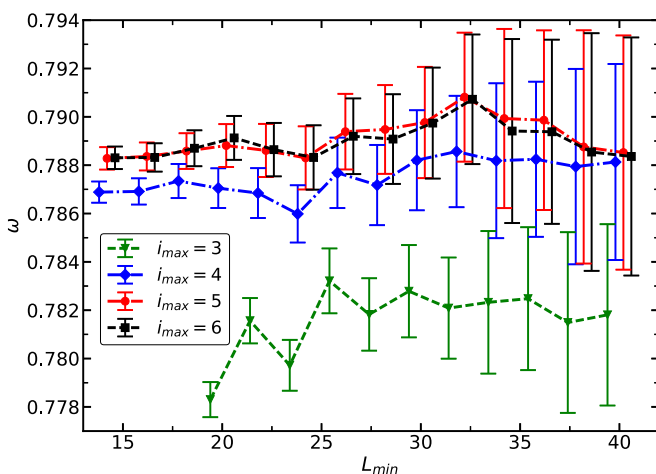


FIG. 5. We plot the estimates of the correction exponent ω obtained by fitting U_4 at $Z_a/Z_p = 0.32037$ using the ansatz (57), where all linear lattice sizes with $L_{\min} \leq L$ are included. Data for $N = 8$ at $D = -0.7, -0.5, 0.0, 0.45, 0.9, 1.02, 1.05, 1.07, 1.24,$ and ∞ are taken into account. The lines connecting the data points should only guide the eye. The L_{\min} are slightly shifted for different fits to make the figure readable.

$i_{\max} = 5$ and 6 at $L_{\min} = 22$. Performing a similar analysis for U_6 at $Z_a/Z_p = 0.32037$, we arrive at $\omega = 0.7880(11)$.

As a check, we have repeated the analysis including fewer values of D : $D = 0.45, 0.9, 1.02, 1.05, 1.07, 1.24,$ and ∞ . Note that for $D = 0.45$ the amplitude of leading corrections to scaling is, up to the sign, roughly the same as for $D = \infty$. Since we have skipped the data with a large amplitude of corrections to scaling, already fits with $i_{\max} = 2$ are consistent with fits using $i_{\max} = 3$. As intermediate results, we quote $\omega = 0.7896(8)$ for U_4 and $L_{\min} = 18$ and $\omega = 0.7886(8)$ for U_6 and $L_{\min} = 18$.

Next, we analyzed U_4 and U_6 at $\xi_{2\text{nd}}/L = 0.59238$. Our intermediate results for ω are slightly smaller than those obtained above. Furthermore, we see a stronger dependence of the results on L_{\min} .

Taking all 10 values of D and $L_{\min} = 26$, we get $\omega = 0.7870(14)$ for U_4 and $0.7862(14)$ for U_6 as intermediate result. Using only $D \geq 0.45$, we get $\omega = 0.7883(21)$ for $L_{\min} = 30$ from U_4 and $i_{\max} = 2$. Based on U_6 , we arrive at $\omega = 0.7875(20)$.

As our final value, we quote

$$\omega = 0.789(4). \quad (58)$$

The central value is mainly given by the results obtain from U_4 and U_6 at $Z_a/Z_p = 0.32037$, since here the estimates depend less on L_{\min} than it is the case for fixing $\xi_{2\text{nd}}/L = 0.59238$. The error bar is chosen such that also the intermediate results obtain for fixing $\xi_{2\text{nd}}/L = 0.59238$ are covered.

2. Locating D^*

Next, we estimate the value D^* of D , where leading corrections to scaling vanish. To this end, we focus again on the neighborhood of D^* and include only data for $D = 1.02, 1.05,$ and 1.07 into the analysis. Since the values of $b(D)$ are small, we have omitted terms with $L^{-n\omega}$ and $n \geq 2$. We made no attempt to discriminate the terms $L^{2-\eta}$ and $L^{-\omega_{NR}}$ in our fits. Hence, we used a single term with an exponent $\epsilon_2 \approx 2$. We used the ansätze

$$\bar{U}(L, D) = \bar{U}^* + b(D)L^{-\epsilon_1}, \quad (59)$$

$$\bar{U}(L, D) = \bar{U}^* + b(D)L^{-\epsilon_1} + c(D)L^{-\epsilon_2}, \quad (60)$$

$$\bar{U}(L, D) = \bar{U}^* + b(D)L^{-\epsilon_1} + c(D)L^{-\epsilon_2} + d(D)L^{-\epsilon_3}. \quad (61)$$

Since the values of D differ little, we performed fits where c and d are the same for all values of D . Furthermore, $b(D) = b'(D - D^*)$, where b' and D^* are the free parameters.

First, we analyzed U_4 at $Z_a/Z_p = 0.32037$. We performed fits without subleading corrections, with one subleading correction term and with two subleading correction terms. In the case of one subleading correction term, we used the two choices $\epsilon_2 = 1.962$ and $\epsilon_2 = 2.02$.

Our estimate of the parameter b' for U_4 at $Z_a/Z_p = 0.32037$ and $\epsilon_1 = \omega = 0.789$ fixed is $b' = -0.121(5)$. In Fig. 6, we plot $\bar{U}_4 + 0.121(D - 1.06)L^{-0.789}$. We find that the data for $D = 1.02, 1.05,$ and 1.07 nicely collapse. This fact shows that our approximations of $b, c,$ and d are adequate.

In Fig. 7, we plot estimates of D^* obtained by fitting U_4 at $Z_a/Z_p = 0.32037$ with the ansätze (59)–(61).

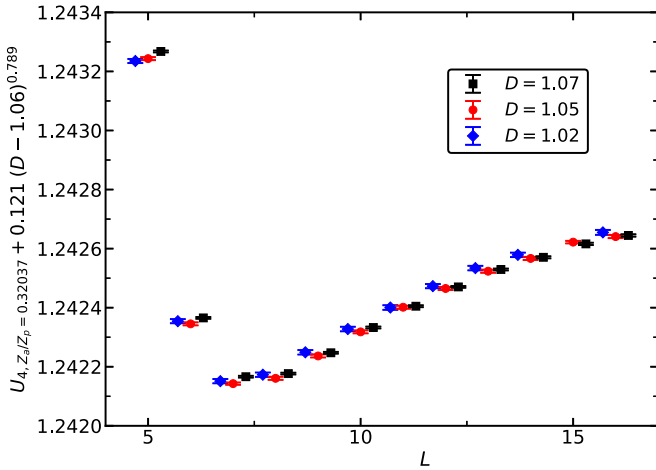


FIG. 6. We plot $U_4(Z_a/Z_p = 0.32037) + 0.121(D - 1.06)L^{-0.789}$ for $N = 8$ at $D = 1.02, 1.05,$ and 1.07 . Note that we have shifted the values of L for $D = 1.02$ and 1.07 to make the figure readable.

Analyzing U_4 at $\xi_{2\text{nd}}/L = 0.59238$, we get a very similar result. Overall, the estimates of D^* are shifted by about 0.005 compared with $Z_a/Z_p = 0.32037$. As our final estimate, we quote

$$D^* = 1.058(13) \quad (62)$$

that covers both the preliminary estimates obtained from fixing $Z_a/Z_p = 0.32037$ and $\xi_{2\text{nd}}/L = 0.59238$. For a discussion of the dependence of D^* on N , see Appendix B 3.

3. The tricritical point

The model undergoes a first-order phase transition for $D < D_{\text{tri}}$. We performed preliminary simulations for a number of $D < D^*$ to roughly locate D_{tri} . In Fig. 8, we plot the Binder cumulant U_4 at $Z_a/Z_p = 0.32037$ for $D = -0.85, -0.86,$ and

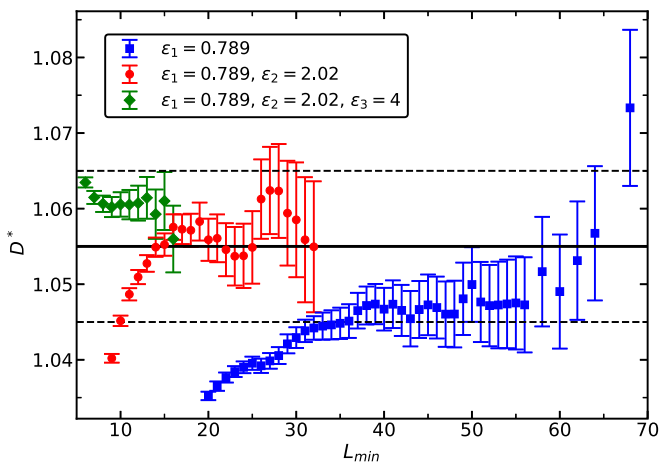


FIG. 7. We plot estimates of D^* obtained from fits of U_4 at $Z_a/Z_p = 0.32037$ for $N = 8$ at $D = 1.02, 1.05,$ and 1.07 as a function of the minimal lattice size L_{min} taken into account. The ansätze (59)–(61) are used. The corresponding correction exponents are given in the legend. Our preliminary estimate $D^* = 1.055(10)$ is indicated by the straight solid line. The dashed lines give the error bar.

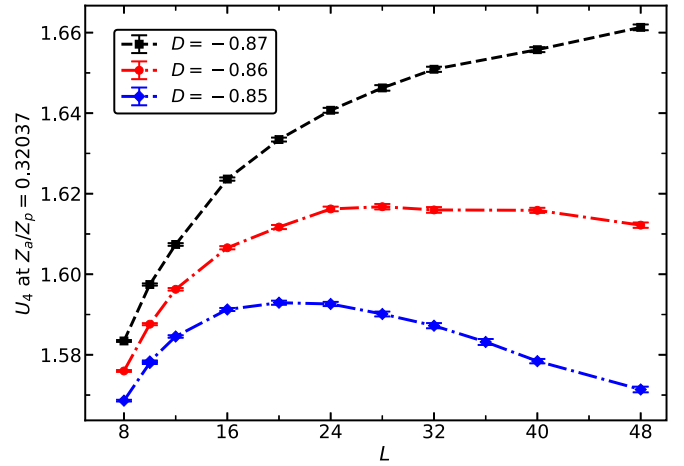


FIG. 8. We plot the Binder cumulant U_4 at $Z_a/Z_p = 0.32037$ for $N = 8$ at $D = -0.85, -0.86,$ and -0.87 for linear lattice sizes $8 \leq L \leq 48$. The lines connecting the data points should only guide the eye.

-0.87 , which are close to our preliminary estimate of D_{tri} . For $D = -0.87$, the Binder cumulant is increasing with increasing lattice size for the lattice sizes studied. It seems plausible that this behavior extends to larger lattice sizes. In contrast, for $D = -0.86$, and more clearly for -0.85 , the Binder cumulant increases for small lattice sizes, while it decreases for larger ones. We conclude that $-0.87 < D_{\text{tri}} < -0.86$.

C. The critical exponent ν

We compute the exponent $\nu = 1/y_t$ from the derivative of a dimensionless quantity R_j with respect to β at a fixed value of a second quantity R_i , where R_j and R_i might be the same. Following the discussion of Sec. III, these slopes behave as

$$\begin{aligned} \bar{s}_{R,i,j} &= \left. \frac{\partial R_j}{\partial \beta} \right|_{R_i=R_{i,f}} \\ &= aL^{y_t} [1 + bL^{-\omega} + \dots + cL^{-\omega_{NR}} + \dots]. \end{aligned} \quad (63)$$

We construct improved slopes by multiplying $\bar{s}_{R,i,j}$ with a certain power p of the Binder cumulant \bar{U}_4 :

$$\bar{s}_{R,\text{imp}} = \bar{s}_R \bar{U}_4^p, \quad (64)$$

where both \bar{s}_R and \bar{U}_4 are taken at $R_{i,f}$. The exponent p is chosen such that, at the level of our numerical accuracy, leading corrections to scaling are eliminated. This idea is discussed systematically in Ref. [25]. To determine p , we consider the pairs $(D_1, D_2) = (0.9, 1.24)$ and $(0.45, \infty)$. These pairs are chosen such that the amplitude of leading corrections has roughly the same modulus, but opposite sign. We fit ratios of $\bar{s}_{R,i,j}$ and \bar{U}_4 with the ansätze

$$\frac{\bar{s}_{R,i,j}(D_1)}{\bar{s}_{R,i,j}(D_2)} = a_S(1 + b_S L^{-\epsilon_1}) \quad (65)$$

and

$$\frac{\bar{U}_4(D_1)}{\bar{U}_4(D_2)} = 1 + b_U L^{-\epsilon_1}, \quad (66)$$

TABLE IV. Numerical result for the exponents p that eliminate leading corrections to scaling in S_R , Eq. (64).

| Fixing \ Slope of | Z_a/Z_p | ξ_{2nd}/L | U_4 | U_6 |
|-------------------------|-----------|---------------|----------|----------|
| $Z_a/Z_p = 0.32037$ | 0.95(3) | 0.30(4) | -2.22(7) | -3.74(7) |
| $\xi_{2nd}/L = 0.59398$ | 0.60(4) | 0.41(4) | -2.36(6) | -3.86(6) |

where we fixed $\epsilon_1 = 0.789$. The exponent p is given by

$$p = -\frac{b_S}{b_U}. \quad (67)$$

In Table IV, we give our final results for p . These are taken from fits for $(D_1, D_2) = (0.9, 1.24)$ and $L_{\min} = 18$. The statistical error is dominated by Eq. (65). In Table IV, we give the statistical error only. Our numerical results obtained for $(D_1, D_2) = (0.45, \infty)$ are consistent. In the case of $(D_1, D_2) = (0.45, \infty)$ we also used fits with one additional correction term. Note that the results for the exponent p change very little when we vary ϵ_1 within the error bars of Eq. (58).

As a check, we have computed the RG exponent y_t for $D = \infty$ using the ansatz $\bar{S}_R = aL^{y_t} (1 + cL^{-2})$. Taking the data for $\bar{S}_{R,imp}$, we get estimates that are consistent with our final result obtained below. In contrast, fitting \bar{S}_R without improvement, the results differ clearly and depend on the dimensionless ratio R that is considered.

1. Statistical errors

In the case of the slopes S_R , we find a moderate reduction of the statistical error when computed at $Z_a/Z_p = 0.32037$ or $\xi_{2nd}/L = 0.59238$ instead of $\beta \approx \beta_c$. It is of the order of a few percent. In contrast, for the magnetic susceptibility that we discuss below, we find a significant reduction. The relative statistical error of the slope of Z_a/Z_p and ξ_{2nd}/L is roughly the same. For U_4 and U_6 for $L = 32$, it is about twice as large as for Z_a/Z_p and ξ_{2nd}/L . With increasing lattice size, this ratio is shrinking. For $L = 512$, roughly a factor of 1.8 remains. In general, there is a degradation with increasing lattice size. For example, the product of statistics times the square of the relative statistical error increases for the slope of ξ_{2nd}/L by a factor of 2.4, going from $L = 32$ to 512. Since we performed a binning of the data during the simulation, we cannot disentangle whether this is due to an increasing autocorrelation time or an increasing variance.

2. Our final estimate of y_t

The idea of using improved derivatives at $D \approx D^*$ is that leading corrections are highly suppressed and they can be ignored safely. In order to obtain our final estimate of ν , we perform joint fits of our data obtained for $D = 1.05$ and $D = 1.07$. We use the ansätze

$$\bar{S}_R = a(D)L^{y_t}, \quad (68)$$

$$\bar{S}_R = a(D)L^{y_t} (1 + cL^{-\epsilon_1}), \quad (69)$$

where $\epsilon_1 \approx 2$. This choice is motivated by the fact that we expect corrections with the exponents $2 - \eta$, $\omega_R \approx 2.02$, and

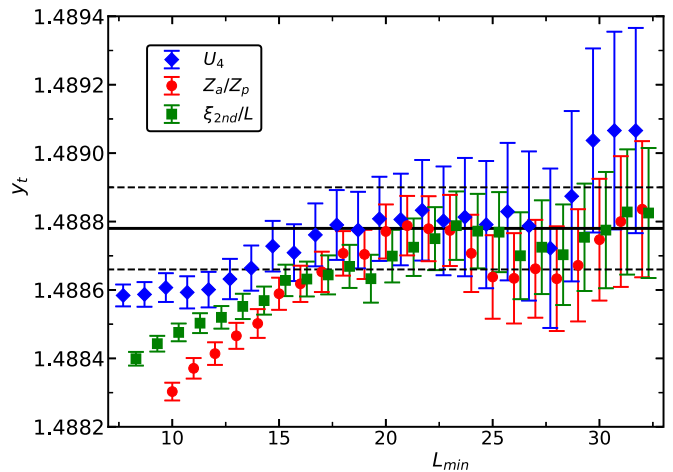


FIG. 9. Estimates of the RG exponent y_t obtained from fitting the improved slopes of U_4 , Z_a/Z_p , and ξ_{2nd}/L at $\xi_{2nd}/L = 0.59238$ for $N = 8$ at $D = 1.05$ and 1.07 as a function of the minimal linear lattice size L_{\min} that is taken into account. The ansatz (69) is used. To make the figure readable, we shifted the values of L_{\min} by -0.3 and 0.3 , for two of the fits. The straight solid line gives our preliminary estimate obtained from the improved slopes at $\xi_{2nd}/L = 0.59238$. The dashed lines indicate our preliminary error estimate.

$-y_t + \omega \approx 2.278$ and larger ones. Our final estimates are based on fits with a single correction exponent.

In Fig. 9, we give the results of such fits for fixing $\xi_{2nd}/L = 0.59238$. The results obtained from the slope of U_6 are not plotted, since they are similar to those of U_4 . For Z_a/Z_p , we get $\chi^2/\text{d.o.f} = 0.871$ with $L_{\min} = 15$. For ξ_{2nd}/L , we get $\chi^2/\text{d.o.f} = 1.000$ with $L_{\min} = 20$. For U_4 , we get $\chi^2/\text{d.o.f} = 0.815$ already for $L_{\min} = 7$. The estimates of y_t obtained from the improved slopes of the three different quantities are consistent starting from $L_{\min} \approx 18$. Furthermore, the estimates are increasing with increasing L_{\min} up to about $L_{\min} = 23$. For $L_{\min} = 23$, from the slopes of Z_a/Z_p and ξ_{2nd}/L we read off our preliminary result, $y_t = 1.48878(12)$.

In Fig. 10, we give the results of such fits for fixing $Z_a/Z_p = 0.32037$. In the case of ξ_{2nd}/L , we get $\chi^2/\text{d.o.f} = 1.064$ for $L_{\min} = 15$. For Z_a/Z_p , we get $\chi^2/\text{d.o.f} = 0.963$ with $L_{\min} = 10$. In the case of U_4 , we get $\chi^2/\text{d.o.f} = 0.899$ for $L_{\min} = 8$. Despite this fact, fully consistent results for y_t among the three quantities are only reached for $L_{\min} \approx 23$. Our preliminary result $y_t = 1.48880(13)$ is based on the fits of the slope of Z_a/Z_p and ξ_{2nd}/L for $L_{\min} = 23$. In Fig. 10, it is indicated by a straight line. The dashed lines give our estimate of the error.

Taking into account both the results from fixing $\xi_{2nd}/L = 0.59238$ and $Z_a/Z_p = 0.32037$, we arrive at

$$y_t = 1.48879(14). \quad (70)$$

The error bar covers both preliminary estimates, including their respective error bars. For the critical exponent of the correlation length, we quote $\nu = 0.67169(7)$. We repeated the fits using the ansatz (69) for fixing $Z_a/Z_p = 0.32$ and 0.321 , $\xi_{2nd}/L = 0.592$, and $\xi_{2nd}/L = 0.593$. The variation of the results for y_t is well below the error quoted in Eq. (70).

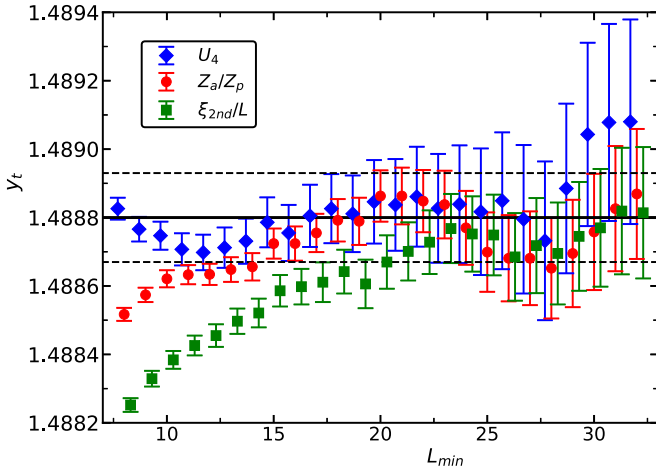


FIG. 10. Estimates of the RG exponent y_t obtained from fitting the improved slopes of U_4 , Z_a/Z_p , and ξ_{2nd}/L at $Z_a/Z_p = 0.32037$ for $N = 8$ at $D = 1.05$ and 1.07 as a function of the minimal linear lattice size L_{min} that is taken into account. The ansatz (69) is used. To make the figure readable, we shifted the values of L_{min} by -0.3 and 0.3 , for two of the fits. The straight lines indicate our preliminary result and its error estimate.

Finally, in Fig. 11, we show results obtained from fits without corrections (68). Here, we have fixed $\xi_{2nd}/L = 0.59238$. Fixing $Z_a/Z_p = 0.32037$ gives similar results. We see that the different estimates of y_t become consistent starting from $L_{min} \gtrsim 60$. As an estimate, we read off $y_t = 1.48875(45)$ corresponding to $\nu = 0.6717(2)$, which is consistent with the estimate given above, Eq. (70), but less precise.

D. The energy density at the critical point

We analyzed the energy density, Eq. (12), at our estimates of β_c for $D = 1.05$ and 1.07 . Here, we do not consider a

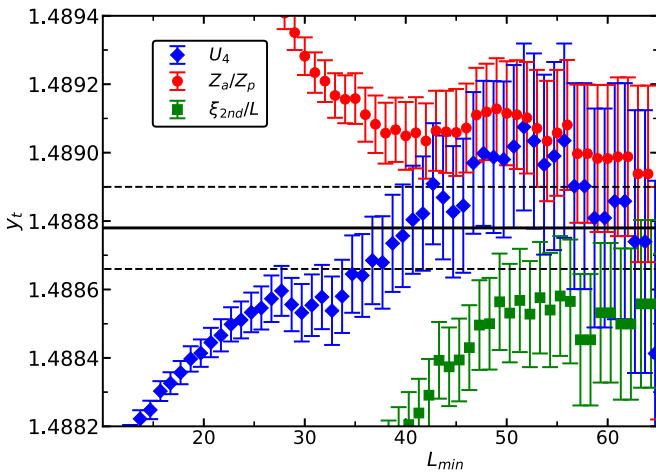


FIG. 11. Estimates of the RG exponent y_t obtained from fitting the improved slopes of U_4 , Z_a/Z_p , and ξ_{2nd}/L at $\xi_{2nd}/L = 0.59238$ for $N = 8$ at $D = 1.05$ and 1.07 as a function of the minimal linear lattice size L_{min} that is taken into account. The ansatz (68) is used. To make the figure readable, we shifted the values of L_{min} by -0.3 and 0.3 , for two of the slopes.

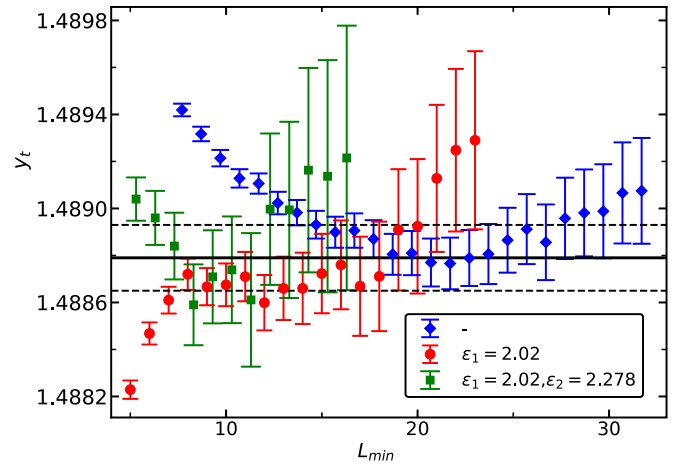


FIG. 12. Estimates for y_t obtained from analyzing the energy density. We fitted the data by using the ansätze (71)–(73). The corresponding correction exponents are given in the legend. L_{min} is the minimal linear lattice size that is included in the fits. Data for $N = 8$ at $D = 1.05$ and 1.07 are taken into account. For comparison, we give the estimate of y_t obtained in the previous section by a straight solid line. The dashed lines give the error bar.

fixed value of Z_a/Z_p or ξ_{2nd}/L since this would generate contributions $\propto (\beta_f - \beta_c)$ from the analytic background of the energy density. Based on Eq. (29), we fitted our data by using the ansätze

$$E = E_0 + aL^{-d+y_t}, \quad (71)$$

$$E = E_0 + aL^{-d+y_t} (1 + cL^{-\epsilon_1}), \quad (72)$$

$$E = E_0 + aL^{-d+y_t} (1 + cL^{-\epsilon_1} + dL^{-\epsilon_2}), \quad (73)$$

where $\epsilon_1 = 2.02$ and $\epsilon_2 = y_t + \omega \approx 2.278$. In our joint fits for $D = 1.05$ and 1.07 , $E_0(1.05)$ and $E_0(1.07)$ are both free parameters of the fit. The same holds for $a(1.05)$ and $a(1.07)$. In contrast, we set $c(1.05) = c(1.07)$ and $d(1.05) = d(1.07)$. In the case of the ansatz (71), we find $\chi^2/\text{d.o.f.} = 0.680$ for $L_{min} = 15$. In the case of the ansatz (72), we get $\chi^2/\text{d.o.f.} = 0.798$ for $L_{min} = 8$. For the ansatz (73), we get $\chi^2/\text{d.o.f.} = 0.931$ with $L_{min} = 5$. Our results for the RG exponent y_t are shown in Fig. 12. For comparison, we give the result obtained in the previous section by the solid horizontal line. The estimates of y_t obtained from the energy density are consistent with those obtained from the slopes of dimensionless ratios but a little less precise. Therefore, we abstain from giving a final estimate of y_t based on the analysis of this section.

E. Exponent η from the behavior of the magnetic susceptibility χ

As observed in previous work [21], we find that the statistical error of χ is reduced, when computed at a fixed value of a phenomenological coupling compared with the error at a given value of $\beta \approx \beta_c$. Comparing U_4 , Z_a/Z_p , and ξ_{2nd}/L , we find that the reduction is clearly the largest for fixing $\xi_{2nd}/L = 0.59238$. For example, for $D = 1.07$ and $L = 512$ we find a reduction of the statistical error by a factor of about 3.3 compared with χ at $\beta = 0.55888340$. This factor is slowly increasing with increasing lattice size.

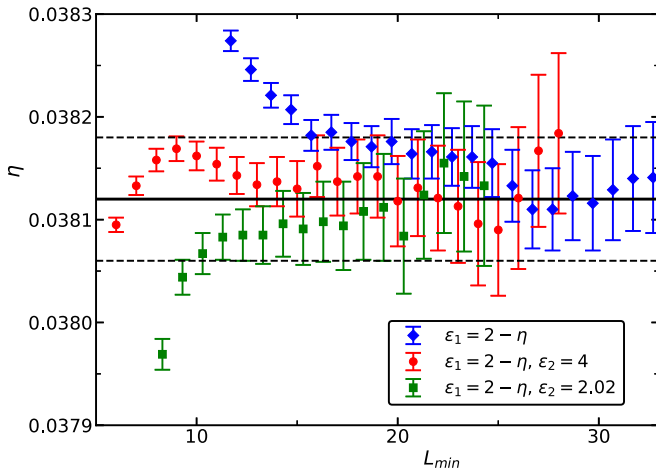


FIG. 13. Estimates of the critical exponent η obtained from fitting the improved magnetic susceptibility χ_{imp} at $Z_a/Z_p = 0.32037$ for $D = 1.05$ and 1.07 as a function of the minimal linear lattice size L_{min} that is taken into account. The ansätze (76) and (77) are used. To make the figure readable, we shifted the values of L_{min} by -0.3 and 0.3 , for two of the fits.

Also, here we analyzed the improved quantities

$$\bar{\chi}_{imp} = \bar{\chi} \bar{U}_4^p, \quad (74)$$

where both χ and U_4 are taken either at $Z_a/Z_p = 0.32037$ or $\xi_{2nd}/L = 0.59238$. We computed the exponent p in a way similar to that in the previous section for S_R . Therefore, we skip a detailed discussion and only report our results: $p = -0.97(2)$ and $-0.45(1)$ for $Z_a/Z_p = 0.32037$ and $\xi_{2nd}/L = 0.59238$, respectively.

We fitted our data with the ansätze

$$\bar{\chi}_{imp} = aL^{2-\eta}, \quad (75)$$

$$\bar{\chi}_{imp} = aL^{2-\eta} + b, \quad (76)$$

$$\bar{\chi}_{imp} = aL^{2-\eta}(1 + cL^{-\epsilon_2}) + b. \quad (77)$$

In the case of Eq. (77), we fixed either $\epsilon_2 = 2.02$ or $\epsilon_2 = 4$.

Let us first discuss the analysis of the data for $Z_a/Z_p = 0.32037$ fixed. In Fig. 13, we plot our estimates of η obtained by using the ansätze (76) and (77). In Fig. 13, the analytic background is indicated by $\epsilon_1 = 2 - \eta$. In the case of ansatz (76), we find $\chi^2/\text{d.o.f.} = 0.899$ for $L_{min} = 16$. For the ansatz (77), $\chi^2/\text{d.o.f.}$ is less than one starting from $L_{min} = 11$ and 8 for $\epsilon_2 = 2.02$ and $\epsilon_2 = 4$, respectively. As our preliminary estimate, we take $\eta = 0.03812(6)$. Fitting without correction term, Eq. (75), $\chi^2/\text{d.o.f.} = 0.95$ is reached for $L_{min} = 40$. However, the estimates of η are further increasing with increasing L_{min} . For $L_{min} = 96$, the estimates seem to level off. We get $\eta = 0.03813(15)$ for $L_{min} = 96$.

Next, we turn to $\xi_{2nd}/L = 0.59238$. In Fig. 14, we plot our estimates of η obtained by using the ansätze (76) and (77). In the case of ansatz (76), we find $\chi^2/\text{d.o.f.} = 1.053$ for $L_{min} = 18$. For the ansatz (77), $\chi^2/\text{d.o.f.}$ is approximately one starting from $L_{min} = 18$ and 14 for $\epsilon_2 = 2.02$ and $\epsilon_2 = 4$, respectively. As our preliminary estimate, we take $\eta = 0.03808(3)$. Fitting without correction term, Eq. (75),

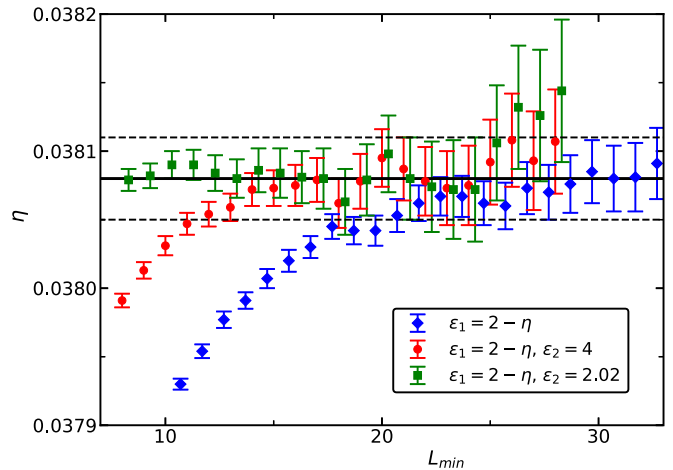


FIG. 14. Estimates of the critical exponent η obtained from fitting the improved magnetic susceptibility χ_{imp} at $\xi_{2nd}/L = 0.59238$ for $D = 1.05$ and 1.07 as a function of the minimal linear lattice size L_{min} that is taken into account. The ansätze (76) and (77) are used. To make the figure readable, we shifted the values of L_{min} by -0.3 and 0.3 , for two of the fits.

$\chi^2/\text{d.o.f.} = 1.336$ is reached for $L_{min} = 64$. For $L_{min} = 96$, we get $\eta = 0.03808(7)$.

We also analyzed the data for χ without improvement, Eq. (74). We do not report the results in detail. They are consistent with those reported above.

As our final result, we quote

$$\eta = 0.03810(8), \quad (78)$$

which is chosen such that the results obtained by using the ansätze (76) and (77) for fixing $Z_a/Z_p = 0.32037$ and $\xi_{2nd}/L = 0.59238$ are covered. As the last check, we repeated the fits using the ansatz (76) for fixing $Z_a/Z_p = 0.32$ and 0.321 , $\xi_{2nd}/L = 0.592$, and $\xi_{2nd}/L = 0.593$. The variation of the results for η is well below the error quoted in Eq. (78).

VI. SUMMARY AND CONCLUSIONS

We have studied a generalized clock model on the simple cubic lattice by using a finite-size scaling analysis. In the case of the N -state clock model, for $N \geq 5$, at the critical point, with increasing length scale, the Z_N symmetry is enhanced to $O(2)$; see, for example, Ref. [6]. In the generalized model, denoted by $(N + 1)$ -state clock model, $(0,0)$ is added as allowed value of the spin. The parameter D , which controls the relative weight of $(0,0)$, can be tuned such that the amplitude of leading corrections to scaling vanishes. We were aiming at accurate estimates of critical exponents for the three-dimensional XY universality class. Our motivation to study the $(N + 1)$ -state clock model is that the simulation requires less computer processing time and less memory than that of a model with $O(2)$ symmetry at the microscopic level.

In the main part of our study, we considered $N = 8$. The RG exponent related with a Z_8 symmetric perturbation of the $O(2)$ invariant fixed point takes the value $y_{N=8} = -5.278(9)$ [5]. Hence, deviations from $O(2)$ symmetry vanish rapidly with increasing lattice size and can be ignored in the finite-size

analysis of the data. For $N = 8$, we find even for critical temperatures, which depend on the microscopic details of the model, only little differences compared with the $N \rightarrow \infty$ limit. For a detailed discussion, see Appendix B. In total, we have spend the equivalent 50 years of computer processing time on a single core of a Intel Xeon CPU E3-1225 v3 running at 3.20 GHz.

Simulating the model for a large range of the parameter D , we determined the exponent of the leading correction $\omega = 0.789(4)$ accurately. We located the tricritical point in the phase diagram. The corresponding $-0.87 < D_{\text{tri}} < -0.86$ is clearly smaller than $D^* = 1.058(13)$, where the amplitude of the leading correction vanishes. Focusing on the neighborhood of D^* , we obtain $\eta = 0.03810(8)$ and $\nu = 0.67169(7)$, which are consistent with but more accurate than previous Monte Carlo results [12,13]. The discrepancy with the experiments on the λ transition of ${}^4\text{He}$ [8–10] is not dissolved.

We determined the inverse of the critical temperature β_c for various values of D accurately. This is important information for future studies. We plan to compute two- and three-point functions at criticality on large lattices, similar to what was done in Ref. [28], in order to get estimates for operator product expansion coefficients.

One might also study the low-temperature phase of the improved $(N + 1)$ -state clock model. The consequences of the fact that a Z_N -symmetric perturbation of the $O(2)$ symmetric fixed point is dangerously irrelevant in the low-temperature phase are debated in the literature, as can be seen in Ref. [45] and references therein.

ACKNOWLEDGMENT

This work was supported by the DFG under Grant No. HA 3150/5-1.

APPENDIX A: THE INVERSE CRITICAL TEMPERATURE FOR $N = 8$

Here, we compute β_c for those values of D that are not considered in Sec. V A. To this end, we analyze the behavior of Z_a/Z_p and $\xi_{2\text{nd}}/L$. We fit our data with the ansätze

$$R(\beta_c) = R^* + bL^{-\epsilon}, \quad (\text{A1})$$

$$R(\beta_c) = R^* + bL^{-\epsilon} + cL^{-2\epsilon}, \quad (\text{A2})$$

$$R(\beta_c) = R^* + bL^{-\epsilon} + cL^{-2\epsilon} + dL^{-3\epsilon}, \quad (\text{A3})$$

using $\epsilon = 0.789$. As in Sec. V A, we compute $R(\beta)$ by using its Taylor expansion around β_s up to the third order. The free parameters of the fits are β_c , b , c , and d . R^* is fixed by the numerical results obtained in Sec. V A. Our results for $Z_a/Z_p = 0.32037$ are summarized in Table V. The results obtained for $\xi_{2\text{nd}}/L = 0.59238$ are compatible.

APPENDIX B: THE N DEPENDENCE OF THE INVERSE CRITICAL TEMPERATURE AND D^*

1. The Caley tree

In order to get a first idea, we have computed numerically β_c for the model put on a Caley tree with the coordination number $z = 6$. The phase transition is of mean-field type.

TABLE V. We give our numerical result for the inverse critical temperature β_c for $N = 8$ at the values of D not considered in Sec. V A. Here, we use $(Z_a/Z_p)^* = 0.32037(6)$. The number given in [] is the error due to the uncertainty of $(Z_a/Z_p)^*$.

| D | β_c |
|----------|---------------------|
| ∞ | 0.45416467(10) [7] |
| 1.24 | 0.54365020(30) [10] |
| 0.9 | 0.57645235(30) [11] |
| 0.45 | 0.63625739(10) [8] |
| 0.0 | 0.7191494(3) [1] |
| -0.5 | 0.8423571(7) [1] |
| -0.7 | 0.9008977(10) [1] |

However, β_c for the Caley tree should be a better approximation of β_c for the three-dimensional model than simple mean field.

For given values of D and $\beta > \beta_c$, we computed the magnetization. Estimates of the inverse critical temperature are obtained by solving

$$m = c(\beta - \beta_c)^{1/2} \quad (\text{B1})$$

for two different values of β with respect to c and β_c . Iteratively, we diminish $\beta - \beta_c$ until corrections to Eq. (B1) can be ignored. This way, we obtain the critical temperature up to about 10 accurate digits.

We computed β_c for $D = \infty, 1.0$, and 0.0 and $N = 5, 6, \dots, 12$. Our results are given in Table VI. We find that, at the level of our precision, the results are identical starting from $N = 10$ for $D = \infty$ and $D = 1$. For $D = 0$, this holds starting from $N = 11$. Deviations from the limit $N \rightarrow \infty$ seem to increase with decreasing D . The approach $N \rightarrow \infty$ is compatible with an exponential decay with a large, D -dependent, decay rate.

2. N dependence of β_c : Three-dimensional model

We performed simulations for $N \neq 8$ for a small number of lattice sizes. We determined $\beta_{f, Z_a/Z_p=0.32037}$, where $Z_a/Z_p = 0.32037$, and $\beta_{f, \xi_{2\text{nd}}/L=0.59238}$, where $\xi_{2\text{nd}}/L = 0.59238$. Since the difference of β_c for different values of N is essentially related to the microscopic details of the model at small scales, we expect that differences or ratios of β_f obtained for moderate lattice sizes are good approximations of the differences or ratios of β_c . Note that Z_a/Z_p is only defined for even values of

TABLE VI. We give our numerical result for the inverse critical temperature $\beta_{c, \text{Caley}}$ for the Caley tree with coordination number $z = 6$.

| $N \setminus D$ | ∞ | 1 | 0 |
|-----------------|--------------|--------------|--------------|
| 5 | 0.4081307306 | 0.5224090169 | 0.6890295689 |
| 6 | 0.4082712294 | 0.5227444788 | 0.6898803344 |
| 7 | 0.4082770202 | 0.5227621638 | 0.6899394147 |
| 8 | 0.4082772183 | 0.5227629375 | 0.6899428166 |
| 9 | 0.4082772241 | 0.5227629665 | 0.6899429844 |
| 10 | 0.4082772243 | 0.5227629675 | 0.6899429916 |
| 11 | 0.4082772243 | 0.5227629675 | 0.6899429919 |
| 12 | 0.4082772243 | 0.5227629675 | 0.6899429919 |

TABLE VII. We give our numerical estimates for the ratio $r = \beta_{c,N=8}/\beta_{c,N}$ obtained from $\beta_{f,Z_a/Z_p=0.32037}$ and $\beta_{f,\xi_{2nd}/L=0.59238}$. In addition, results based on Ref. [45] are reported.

| D | N | $Z_a/Z_p = 0.32037$ | $\xi_{2nd}/L = 0.59238$ | Ref. [45] |
|----------|-----|---------------------|-------------------------|-------------|
| ∞ | 5 | | | 1.001442(5) |
| ∞ | 6 | 1.00007847(22) | 1.00007837(20) | 1.000075(5) |
| ∞ | 7 | | 1.00000362(21) | |
| ∞ | 10 | 1.00000015(21) | 0.99999984(20) | |
| 1.07 | 6 | 1.00017147(32) | 1.00017141(29) | |
| 1.07 | 7 | | 1.00000946(15) | |
| 1.07 | 12 | 0.99999938(16) | 0.99999947(16) | |
| 1.02 | 6 | 1.0001772(3) | 1.0001769(3) | |

N . We study the ratio

$$r(L) = \frac{\beta_{f,N=8}(L)}{\beta_{f,N}(L)}. \quad (\text{B2})$$

As discussed in Sec. III, there is an N dependence of all scaling fields. In particular, there should be a dependence, albeit small, of the scaling field related to the leading correction to scaling. Therefore, we expect that

$$r(L) = \frac{\beta_{c,N=8}}{\beta_{c,N}} + cL^{-\epsilon} + \dots \quad (\text{B3})$$

where $\epsilon = 1/\nu + \omega$ is the exponent related with the leading correction. We performed simulations for $D = \infty$, 1.07, and $D = 1.02$. Let us first discuss our results for $D = \infty$. For $N = 6$, we simulated the linear lattice sizes $L = 32, 36$, and 40. The ratios, Eq. (B2), for these three lattice sizes are consistent within their error bars. The average is given in Table VII. For $N = 7$, we simulated the lattice sizes $L = 36$ and 40. For $N = 10$, we simulated the lattice sizes $L = 32, 40$, and 48. Also for these two values of N , the averages are given in Table VII. In addition, we make use of the estimates $1/\beta_{c,N=5} = 2.20502(1)$ and $1/\beta_{c,N=6} = 2.20201(1)$ reported in Ref. [45]. Note that for $N = 6$, the result of Ref. [45] is fully consistent with ours. Similar to the Caley tree approximation, we see a rapid convergence of $\beta_{c,N}$ with $N \rightarrow \infty$. Already for $N = 8$ and 10, we cannot find a difference at our level of accuracy. Extrapolating the ratios for smaller values of N , we get $\beta_{c,N=8}/\beta_{c,9} \approx 0.99999985$. At our level of precision, the same ratio holds for all $N \geq 9$. Using this estimate, we arrive at $\beta_{c,XY} = 0.45416474(10)$ [7]. In Table VIII, we summarize estimates of $\beta_{c,XY}$ given in the literature.

Next, let us discuss the results for $D = 1.07$. Here, we simulated the linear lattice sizes $L = 64$ for $N = 6$, $L = 32, 40, 48$, and 64 for $N = 7$ and $L = 48$ and 64 for $N = 12$. The averages of the ratios of β_f are reported in Table VII. Similar to $D = \infty$, we see a rapid convergence of $\beta_{c,N}$, which is, however, slightly slower than it is the case for $D = \infty$. In particular, our estimate for $\beta_{c,N=8}/\beta_{c,N=12}$ differs from 1 by about 3.6 times the error bar. Extrapolating the results for $N < 8$, we arrive at $\beta_{c,N=8}/\beta_{c,N>8} \approx 0.99999995$.

Finally, for $D = 1.02$, we have simulated $L = 4, 5, \dots, 14, 16, 18, 20$, and 64 for $N = 6$. These simulations were performed at an early stage of the study, mainly to determine the correction exponent y_6 . Here, we see a dependence of the

TABLE VIII. We summarize results from the literature for the inverse critical temperature of the XY model on the simple cubic lattice.

| Ref. | Year | β_c |
|-----------|------|-------------------|
| [46] | 2005 | 0.4541655(10) |
| [12] | 2006 | 0.4541652(5)[6] |
| [47] | 2012 | 0.45416313(20) |
| [47] | 2012 | 0.45416742(12) |
| [37] | 2014 | 0.4541664(12) |
| [13] | 2019 | 0.45416466(10) |
| This work | 2019 | 0.45416474(10)[7] |

ratio r , Eq. (B2), on the lattice size L . First, we analyzed the results obtained for $\beta_{f,Z_a/Z_p=0.32037}$. We fitted our data with the ansatz

$$r(L) = a + cL^{-\epsilon}, \quad (\text{B4})$$

using the numerical value $\epsilon = 1/\nu + \omega = 2.27779$. Including data with $L \geq 8$, we get $a = 1.0001772(3)$, $c = 0.00155(12)$, and $\chi^2/\text{d.o.f.} = 0.70$. The analysis of the data for $\beta_{f,\xi_{2nd}/L=0.59238}$ gives very similar results. Our final estimates are given in Table VII.

3. N dependence of D^*

As discussed in Sec. III, the value of D^* depends on N . To get a numerical estimate, we analyze the Binder cumulant \bar{U}_4 at either $Z_a/Z_p = 0.32037$ or $\xi_{2nd}/L = 0.59238$ at values of D close to D^* .

First, we estimate the slope of the correction amplitude close to D^* for $N = 8$ by fitting the data with the ansatz

$$\bar{U}_4(N = 8, D = 1.07) - \bar{U}_4(N = 8, D = 1.02) = b_d L^{-\omega}, \quad (\text{B5})$$

where we have fixed $\omega = 0.789$, or

$$\begin{aligned} \bar{U}_4(N = 8, D = 1.07) - \bar{U}_4(N = 8, D = 1.02) \\ = b_d L^{-\omega} + c_d L^{-2}. \end{aligned} \quad (\text{B6})$$

In the following, we assume that the dependence of

$$\left. \frac{db}{dD} \right|_{D=D^*} \approx \frac{b_d}{0.05} \quad (\text{B7})$$

on N can be ignored. We get $b_d = -0.00616(10)$ for fixing $Z_a/Z_p = 0.32037$ and $b_d = -0.00705(16)$ for fixing $\xi_{2nd}/L = 0.59238$.

In the second step, we analyze how \bar{U}_4 changes with N at a fixed value of D . To this end, we define

$$\Delta_U(N_1, N_2, D) = \bar{U}_4(N_1, D) - \bar{U}_4(N_2, D), \quad (\text{B8})$$

where here $N_2 = 8$. We fitted our data with the ansätze

$$\Delta_U(N_1, N_2, D) = \Delta_b(N_1, N_2, D)L^{-\omega}, \quad (\text{B9})$$

where we have fixed $\omega = 0.789$ and

$$\Delta_U(N_1, N_2, D) = \Delta_b(N_1, N_2, D)L^{-\omega} + \Delta_c(N_1, N_2, D)L^{-\epsilon}, \quad (\text{B10})$$

where we fixed $\epsilon = 2$. In the case of $N_1 = 6$, we used in addition $\epsilon = 2.4$. The shift in D^* is given by

$$D^*(N_1) - D^*(8) \approx -\Delta_b(N_1, 8, D) \frac{0.05}{b_d}. \quad (\text{B11})$$

For the purpose of this section, we have simulated the linear lattice size $L = 4, 5, 6, \dots, 16$ for $N = 10$ at $D = 1.07$ with a statistics similar to that for $N = 8$. It turns out that $\Delta_U(10, 8, 1.07)$ is compatible with zero for most of the lattice sizes. Fitting the data for $L \geq 8$ with the ansatz (B9), we get $\Delta_b(10, 8, 1.07) = -0.000004(10)$ and $-0.000012(10)$ for fixing $Z_a/Z_p = 0.32037$ and $\xi_{2\text{nd}}/L = 0.59238$, respectively. Fitting with the ansatz (B10), the estimates stay compatible with zero, but with a larger error bar. Taking also these results into account, we conclude that $|D^*(10) - D^*(8)| \lesssim 0.0005$.

Next, we have analyzed our data for $N = 6$ and $D = 1.02$. Taking into account the results of the fits using different ansätze, we arrive at $\Delta_b(6, 8, 1.02) = 0.00163(6)$ for fixing $Z_a/Z_p = 0.32037$ and $\Delta_b(6, 8, 1.02) = 0.00198(13)$ for fixing $\xi_{2\text{nd}}/L = 0.59238$. Plugging in the numbers into Eq. (B11), we arrive at $D^*(6) - D^*(8) = 0.0132(5)$ and $0.0140(10)$, for fixing $Z_a/Z_p = 0.32037$ or $\xi_{2\text{nd}}/L = 0.59238$, respectively. As our final result, we take

$$D^*(6) - D^*(8) = 0.0136(14), \quad (\text{B12})$$

covering both the results for fixing $Z_a/Z_p = 0.32037$ and for fixing $\xi_{2\text{nd}}/L = 0.59238$.

Assuming that $D^*(N)$ converges rapidly to $D^*(\infty)$, we conclude that $|D^*(N) - D^*(8)|$ for $N > 8$ is much smaller than the error of $D^*(8)$, Eq. (62). It seems plausible that $D^*(7) - D^*(8)$ is smaller than $D^*(6) - D^*(8)$ computed above. Likely $|D^*(5) - D^*(8)|$ is considerably larger than the error of $D^*(8)$ and an effort beyond that of this section is required to obtain an accurate estimate of $D^*(5)$.

4. N dependence of the magnetic susceptibility and the slope of dimensionless quantities

Finally, we have studied the dependence of quantities that we used to compute the critical exponents ν and η on N . In particular, we consider the magnetic susceptibility and the slopes of dimensionless quantities at either $Z_a/Z_p = 0.32037$ or $\xi_{2\text{nd}}/L = 0.59238$. Let us discuss the results obtained for the susceptibility. Those for the slopes of dimensionless quantities are qualitatively the same.

We computed the ratio

$$R_\chi(6, 8) = \frac{\chi(N=6)}{\chi(N=8)} \quad (\text{B13})$$

for either $Z_a/Z_p = 0.32037$ or $\xi_{2\text{nd}}/L = 0.59238$ fixed at $D = 1.02$. Following the discussion of Sec. III, this ratio should behave as

$$R_\chi(6, 8) = a(1 + bL^{-\omega} + \dots), \quad (\text{B14})$$

where all possible types of corrections should appear, and not only those related to the breaking of the $O(2)$ symmetry. We have fitted our data by using a single correction term. In the case of $Z_a/Z_p = 0.32037$, we get the following results:

Using the correction exponent $\epsilon = 0.789$ and $L_{\min} = 6$, we get $a = 1.000187(14)$, $b = 0.00126(8)$, and

$\chi^2/\text{d.o.f.} = 0.36$. Using instead $\epsilon = 2$ and $L_{\min} = 8$, we get $a = 1.000295(9)$, $b = 0.0091(10)$, and $\chi^2/\text{d.o.f.} = 0.56$.

For $\xi_{2\text{nd}}/L = 0.59238$ fixed, we get the following: Using the correction exponent $\epsilon = 0.789$ and $L_{\min} = 8$, we get $a = 1.000222(15)$, $b = -0.00010(11)$, and $\chi^2/\text{d.o.f.} = 0.64$. Using instead $\epsilon = 2$ and $L_{\min} = 4$, we get $a = 1.000219(4)$, $b = -0.00143(13)$, and $\chi^2/\text{d.o.f.} = 0.59$.

We conclude that the ratio (B13) consists of an overall constant that is close to one and corrections with a small amplitude. Since these corrections come with a very small amplitude, it is impossible to assign them clearly to the correction exponents that are theoretically expected.

In the case of $N = 8$ and $N = 10$ at $D = 1.07$, the data barely differ. For example, for χ at $\xi_{2\text{nd}}/L = 0.59238$, we get for $L = 4$ the estimates 17.01708(4) and 17.01707(5), respectively. Therefore, we abstain from any further analysis.

APPENDIX C: THE CORRECTION EXPONENT $y_{N=6}$

We define

$$X_N = \langle \max_j \vec{m} \vec{r}_j \rangle, \quad (\text{C1})$$

$$Y_N = \langle \max_j \vec{m} \vec{p}_j \rangle, \quad (\text{C2})$$

where

$$\vec{r}_j = [\cos(2\pi j/N), \sin(2\pi j/N)], \quad (\text{C3})$$

$$\vec{p}_j = \{\cos[2\pi(j+1/2)/N], \sin[2\pi(j+1/2)/N]\}, \quad (\text{C4})$$

where $j \in \{0, \dots, N-1\}$ and

$$(m^{(0)}, m^{(1)}) = \vec{m} = \sum_x \vec{s}_x \quad (\text{C5})$$

is the magnetization. Now, we consider the quantity

$$q_N = \frac{X_N - Y_N}{X_N + Y_N} \quad (\text{C6})$$

as a measure of the deviation from $O(2)$ invariance. We performed simulations for $N = 6$ and $D = 1.02$ close to our final estimate of $D^*(6) = 1.058(13) + 0.0136(14)$. We simulated the lattice sizes $L = 4, 5, \dots, 16, 18, 20$, and 64, as discussed already above. The quantities X_N and Y_N are taken at $Z_a/Z_p = 0.32037$. Note that q_N for $L = 64$ is equal to zero within error bars. Therefore, we did not include $L = 64$ in our analysis. We fitted our numerical results with the ansätze

$$q_N = cL^{y_{N=6}} \quad (\text{C7})$$

and

$$q_N = cL^{y_{N=6}} \times (1 + bL^{-2}). \quad (\text{C8})$$

We find $y_{N=6} = -2.42(2)$ and $\chi^2/\text{d.o.f.} = 0.53$ with $L_{\min} = 8$ using the first ansatz and $y_{N=6} = -2.46(3)$ and $\chi^2/\text{d.o.f.} = 0.59$ with $L_{\min} = 6$ using the second ansatz. As our final estimate, we take $y_{N=6} = -2.43(6)$, where the error estimate includes the results of both fits.

This value has to be compared with $y_{N=6} = -2.55(6)$ and $-2.509(7)$ given in Refs. [45] and [5], respectively.

Note that for $N > 6$ it is virtually impossible to get a reliable estimate of y_N using the method used here, since the relative error of q_N is rapidly increasing with increasing L .

At a late stage of the project, we have implemented the quantity

$$\phi_N = \langle \cos(N\Theta) \rangle, \quad (\text{C9})$$

where $\Theta = \arccos(m^{(0)}/|\vec{m}|)$, which is used in Ref. [45]; see Eq. (3) of Ref. [45]. We simulated the linear lattice sizes

$L = 4, 6, 8,$ and $12,$ measuring both ϕ_N and q_N . We find that the relative error is slightly smaller for q_N , the two quantities are highly correlated, and their ratio ϕ_N/q_N is within the statistical error the same for the lattice sizes $L = 6, 8,$ and $12.$ For $L = 4,$ it deviates by little. Hence, for our purpose the two quantities are equivalent.

-
- [1] K. G. Wilson and J. Kogut, The renormalization group and the ϵ expansion, *Phys. Rep. C* **12**, 75 (1974).
- [2] M. E. Fisher, The renormalization group in the theory of critical behavior, *Rev. Mod. Phys.* **46**, 597 (1974).
- [3] M. E. Fisher, Renormalization group theory: Its basis and formulation in statistical physics, *Rev. Mod. Phys.* **70**, 653 (1998).
- [4] A. Pelissetto and E. Vicari, Critical phenomena and renormalization-group theory, *Phys. Rept.* **368**, 549 (2002).
- [5] D. Banerjee, S. Chandrasekharan, and D. Orlando, Conformal Dimensions via Large Charge Expansion, *Phys. Rev. Lett.* **120**, 061603 (2018).
- [6] J. Hove and A. Sudbø, Criticality versus q in the (2+1)-dimensional Z_q clock model, *Phys. Rev. E* **68**, 046107 (2003).
- [7] J. Lou, A. W. Sandvik, and L. Balents, Emergence of U(1) Symmetry in the 3D XY Model with Z_q Anisotropy, *Phys. Rev. Lett.* **99**, 207203 (2007).
- [8] J. A. Lipa, D. R. Swanson, J. A. Nissen, T. C. P. Chui, and U. E. Israelsson, Heat Capacity and Thermal Relaxation of Bulk Helium Very Near the λ Point, *Phys. Rev. Lett.* **76**, 944 (1996).
- [9] J. A. Lipa, D. R. Swanson, J. A. Nissen, Z. K. Geng, P. R. Williamson, D. A. Stricker, T. C. P. Chui, U. E. Israelsson, and M. Larson, Specific Heat of Helium Confined to a 57- μm Planar Geometry, *Phys. Rev. Lett.* **84**, 4894 (2000).
- [10] J. A. Lipa, J. A. Nissen, D. A. Stricker, D. R. Swanson and T. C. P. Chui, Specific heat of liquid helium in zero gravity very near the λ -point, *Phys. Rev. B* **68**, 174518 (2003).
- [11] R. Guida and J. Zinn-Justin, Critical exponents of the N vector model, *J. Phys. A* **31**, 8103 (1998).
- [12] M. Campostrini, M. Hasenbusch, A. Pelissetto, and E. Vicari, Theoretical estimates of the critical exponents of the superfluid transition in ^4He by lattice methods, *Phys. Rev. B* **74**, 144506 (2006).
- [13] W. Xu, Y. Sun, J.-P. Lv, and Y. Deng, High-precision Monte Carlo study of several models in the three-dimensional U(1) universality class, *Phys. Rev. B* **100**, 064525 (2019).
- [14] F. Kos, D. Poland, D. Simmons-Duffin, and A. Vichi, Precision islands in the Ising and $O(N)$ models, *J. High Energy Phys.* **08** (2016) 036.
- [15] M. Campostrini, M. Hasenbusch, A. Pelissetto, P. Rossi, and E. Vicari, Critical behavior of the three-dimensional XY universality class, *Phys. Rev. B* **63**, 214503 (2001).
- [16] D. Simmons-Duffin, The lightcone bootstrap and the spectrum of the 3d Ising CFT, *J. High Energy Phys.* **03** (2017) 086.
- [17] J. H. Chen, M. E. Fisher, and B. G. Nickel, Unbiased Estimation of Corrections to Scaling by Partial Differential Approximants, *Phys. Rev. Lett.* **48**, 630 (1982).
- [18] M. E. Fisher and J. H. Chen, The validity of hyperscaling in three dimensions for scalar spin systems, *J. Phys. (Paris)* **46**, 1645 (1985).
- [19] H. W. J. Blöte, E. Luijten, and J. R. Heringa, Ising universality in three dimensions: A Monte Carlo study, *J. Phys. A: Math. Gen.* **28**, 6289 (1995).
- [20] H. G. Ballesteros, L. A. Fernández, V. Martín-Mayor, and A. Muñoz Sudupe, Finite size scaling and “perfect” actions: The three-dimensional Ising model, *Phys. Lett. B* **441**, 330 (1998).
- [21] M. Hasenbusch, K. Pinn, and S. Vinti, Critical exponents of the 3D Ising universality class from finite size scaling with standard and improved actions, *Phys. Rev. B* **59**, 11471 (1999).
- [22] M. N. Barber, in *Finite-Size Scaling in Phase Transitions and Critical Phenomena*, Vol. 8, edited by C. Domb and J. L. Lebowitz (Academic Press, New York, 1983).
- [23] M. Hasenbusch, A Monte Carlo study of leading order scaling corrections of ϕ^4 theory on a three-dimensional lattice, *J. Phys. A* **32**, 4851 (1999).
- [24] M. Hasenbusch and T. Török, High precision Monte Carlo study of the 3D XY-universality class, *J. Phys. A* **32**, 6361 (1999).
- [25] M. Hasenbusch, F. Parisen Toldin, A. Pelissetto, and E. Vicari, Universality class of 3D site-diluted and bond-diluted Ising systems, *J. Stat. Mech.* (2007) P02016.
- [26] M. Hasenbusch, A finite size scaling study of lattice models in the 3D Ising universality class, *Phys. Rev. B* **82**, 174433 (2010).
- [27] K. Binder, Finite size scaling analysis of Ising model block distribution functions, *Z. Phys. B: Condens. Matter* **43**, 119 (1981).
- [28] M. Hasenbusch, Two- and three-point functions at criticality: Monte Carlo simulations of the improved three-dimensional Blume-Capel model, *Phys. Rev. E* **97**, 012119 (2018).
- [29] A. Maciolek, M. Krech, and S. Dietrich, Phase diagram of a model for ^3He - ^4He mixtures in three dimensions, *Phys. Rev. E* **69**, 036117 (2004).
- [30] M. Campostrini, A. Pelissetto, P. Rossi, and E. Vicari, Two-point correlation function of three-dimensional O(N) models: The critical limit and anisotropy, *Phys. Rev. E* **57**, 184 (1998).
- [31] M. Campostrini, A. Pelissetto, P. Rossi, and E. Vicari, 25th-order high temperature expansion results for three-dimensional Ising like systems on the simple cubic lattice, *Phys. Rev. E* **65**, 066127 (2002).
- [32] K. E. Newman and E. K. Riedel, Critical exponents by the scaling-field method: The isotropic N -vector model in three dimensions, *Phys. Rev. B* **30**, 6615 (1984).
- [33] D. F. Litim and L. Vergara, Subleading critical exponents from the renormalisation group, *Phys. Lett. B* **581**, 263 (2004).
- [34] A. Jüttner, D. F. Litim, and E. Marchais, Global Wilson-Fisher fixed points, *Nucl. Phys. B* **921**, 769 (2017).
- [35] U. Wolff, Collective Monte Carlo Updating for Spin Systems, *Phys. Rev. Lett.* **62**, 361 (1989).

- [36] M. Weigel, Simulating spin models on GPU, *Comput. Phys. Commun.* **182**, 1833 (2011).
- [37] Y. Komura and Y. Okabe, CUDA programs for GPU computing of Swendsen-Wang multi-cluster spin flip algorithm: 2D and 3D Ising, Potts, and XY models, *Comput. Phys. Commun.* **185**, 1038 (2014); Improved CUDA programs for GPU computing of Swendsen-Wang multi-cluster spin flip algorithm: 2D and 3D Ising, Potts, and XY models, **200**, 400 (2016).
- [38] M. Saito and M. Matsumoto, SIMD-oriented fast Mersenne twister: A 128-bit pseudorandom number generator, in *Monte Carlo and Quasi-Monte Carlo Methods 2006*, edited by A. Keller, S. Heinrich, and H. Niederreiter (Springer, Berlin, 2008); M. Saito, master's thesis, Hiroshima University, Japan, 2007 (unpublished). The source code of the program is provided at <http://www.math.sci.hiroshima-u.ac.jp/~m-mat/MT/SFMT/index.html>.
- [39] J. D. Hunter, MATPLOTLIB: A 2D graphics environment, *Comput. Sci. Eng.* **9**, 90 (2007).
- [40] T. E. Oliphant, PYTHON for scientific computing, *Comput. Sci. Eng.* **9**, 10 (2007); P. Virtanen, R. Gommers, T. E. Oliphant *et al.*, SciPy 1.0—fundamental algorithms for scientific computing in python, [arXiv:1907.10121](https://arxiv.org/abs/1907.10121).
- [41] K. Levenberg, A method for the solution of certain non-linear problems in least squares, *Quart. Appl. Math.* **2**, 164 (1944).
- [42] D. Marquardt, An algorithm for least-squares estimation of nonlinear parameters, *SIAM J. Appl. Math.* **11**, 431 (1963).
- [43] J. J. Moré, The Levenberg-Marquardt algorithm, *Lecture Notes Math.* **630**, 105 (1978).
- [44] J. J. Moré, B. S. Garbow, and K. E. Hillstom, User guide for MINPACK-1, Argonne National Laboratory Report ANL-80-74, Argonne, IL, 1980; J. J. Moré, D. C. Sorensen, K. E. Hillstom, and B. S. Garbow, The MINPACK project, in *Sources and Development of Mathematical Software*, edited by W. J. Cowell (Prentice-Hall, New York, 1984).
- [45] H. Shao, W. Guo, and A. W. Sandvik, Monte Carlo renormalization flows in the space of relevant and irrelevant operators: Application to three-dimensional clock models, [arXiv:1905.13640](https://arxiv.org/abs/1905.13640) (unpublished).
- [46] Y. Deng, H. W. J. Blöte, and M. P. Nightingale, Surface and bulk transitions in three-dimensional $O(n)$ models, *Phys. Rev. E* **72**, 016128 (2005).
- [47] T.-Y. Lan, Y.-D. Hsieh, and Y.-J. Kao, High-precision Monte Carlo study of the three-dimensional XY model on GPU, [arXiv:1211.0780](https://arxiv.org/abs/1211.0780) (unpublished).